BERKELEY LAB
Earth Sciences Division

AMERIFLUX
MANAGEMENT PROJECT

14 December 2016

Dennis Baldocchi, Siyan Ma, and Joseph Verfaillie
Department of Environmental Science, Policy, and Management
University of California, Berkeley

Dear Dennis, Siyan, and Joe

Thank you very much for hosting the AmeriFlux Tech team site visit at Tonzi Ranch (US-Ton) from 12 – 25 April 2016 (DOY 103-116). This report summarizes the findings and key recommendations from the comparison between the AmeriFlux portable eddy covariance system #2 (PECS2) and the *in situ* system for eddy covariance, radiation, and meteorological observations.

The AmeriFlux PECS2 sensors were deployed to minimize separation (both horizontal and vertical) from the *in situ* sensors (Appendix 1), to avoid interfering with existing infrastructure, and to prevent shadowing or wake effects. The AmeriFlux PECS2 was deployed with two infrared gas analyzers (an enclosed-path - LI-7200, and an open-path analyzer - LI-7500A). Both gas analyzers are calibrated prior to and after each deployment, with this comparison focusing on the AmeriFlux open-path IRGA as it is similar to the *in situ* eddy covariance system. Data processing of the AmeriFlux PECS2 data was handled by EddyPro® (Version 5.2.1), an open-source eddy covariance software package developed by LI-COR (http://licor.com/env/products/eddy_covariance/software.html). We are currently in the process of updating the details of the AmeriFlux data processing and data screening on the AmeriFlux website (ameriflux.lbl.gov). Please contact the AmeriFlux Tech team if you have specific questions.

Four figures are generated for each variable compared. The top figure is a time series of both systems over the evaluation period. The middle figure is a time series of the differences between the systems. The lower left figure is a scatter plot of both systems with the ideal 1 to 1 regression line and the best fit linear regression together with equation and fit parameters. Lastly, the lower right figure is a histogram of the differences between the systems with summary statistics. The enclosed figures only include periods where both datasets are available and quality controlled. Missing data periods occurred when data was screened from one or both systems either through data quality checks, outlier removal, environmental interference (precipitation), or no data (power outage) (Figure 1).

Key Recommendations:

Overall, the comparison between the AmeriFlux PECS2 and the *in situ* system was good. Please see a few key findings highlighted below:

- Though the comparison between the two open-path gas analyzers was relatively good, we noted a clear offset in the water vapor channel of the *in situ* open-path gas analyzer. We recommend carrying out regular calibration checks and calibrations. That said calibrations should be carried out in lab conditions and not on site where ambient conditions might influence the accuracy of the calibration procedure.
- We have observed that the variance of CO_2 to be distinctively different from the PECS2, but also from the independently processed raw *in situ* data. Please verify the calculations behind the *in situ* values as none of the applied processing methods (despiking threshold, detrending, etc.) made it possible for us to reproduce the *in situ* CO_2 variances. Furthermore, we observed the *in situ* covariance between vertical wind and CO_2 to be of a factor of 0.001 of the final estimated CO_2 flux. Please verify calculations or data headers behind these values.
- The provided *in situ* CO_2 mixing ratios show large discrepancies between these and the independently estimated values from raw *in situ* data. These discrepancies were observed during periods when the *in situ* ambient air temperature HMP probe diverted by more than 1°C from the PECS2 HMP probe. The use of the current *in situ* HMP45 probe in the conversion have contributed to these discrepancies as the *in situ* HMP45 probe showed to underreport true values, particularly at night.

- Recorded values from the *in situ* HMP45 probe divert by more than 5°C and by more than 20% (absolute terms) in relative humidity at night. We recommend investigating this by comparing to other temperature measurements carried out at the site. We also recommend such HMP probes to be sent for service and factory calibration (both, temperature and relative humidity) at least every two years in order to guarantee accurate ambient air temperature and relative humidity readings.
- Wind direction estimated with the *in situ* sonic anemometer (Gill-Windmaster Pro) deviates by several degrees when compared to the PECS2 sonic anemometer (Gill R3-50). While on site, the AmeriFlux Tech team measured locations, heights and orientation of both PECS2 and *in situ* instruments. This allows the Tech team to estimate wind direction from *in situ* raw data independently. Please verify orientation of the *in situ* sonic anemometer.
- We observed missing nighttime values for incoming shortwave radiation measured by the CNR1 radiometer. Please consult the data acquisition settings for this channel as net radiation values estimated from this radiometer would be questionable. Therefore, the comparison carried out here includes data from the CNR1 for the individual pyranometer and pyrgeometer channels but net radiation using the NRLite sensor data.

Summarizing, we emphasize regular calibration checks and following the manufacturer's recommendations for routine maintenance (factory calibration, changing internal chemicals, etc.) of gas analyzer and meteorological sensors, and the verification of the implemented conversion and calibration factors when converting to engineering units. Note that the AmeriFlux Tech team provides calibration gases (check and span) as well as calibrated PAR sensors at no cost to active AmeriFlux sites, to conduct their own calibrations.

In closing, thank you for your cooperation before, during, and after the site visit and we encourage you to continue your active participation in the AmeriFlux network. We are actively soliciting comments or feedback regarding the site visit process and report to maximize the utility of our visits. For all reports, we request a summary from the site to describe how the enclosed recommendations will be addressed. We are available to provide further analysis or discussion of the results, if required.

Please review the general site information table in Appendix 1 of this document and let us know if you notice erroneous information. Thank you for working collaboratively with the AmeriFlux Tech team.

All the best,

Sigrid Dengel[1], Stephen Chan[1], Sébastien Biraud[1], David Billesbach[2], Chad Hanson[3]
AmeriFlux Tech team

[1]Lawrence Berkeley National Laboratory
[2]University of Nebraska, Lincoln
[3]Oregon State University

Detailed Report

Data availability:

The PECS2 was deployed from 12 – 25 April 2016 (Figure 1) with observations spanning a total of 12 full days. A few periods of data were excluded from the analysis when the PECS2 leaf wetness sensor (LWS) recorded periods of rain or condensation affecting open-path gas analyzer signal strength and gas mole density readings.

Data processing

The site staff provided the raw 10Hz data from the *in situ* eddy flux setup. Raw *in situ* data were processed in the same manner, applying the same corrections as applied to the PECS2 system and by taking the appropriate site properties in consideration (Appendix 1). We found significant differences in the processing output of the concentration and variance of CO_2 and covariance of vertical wind and CO_2 between *in situ* and independently processed *in situ* data (please see Figure 15 - Figure 17). These differences possibly explain the seen discrepancies between *in situ* and PECS2 values.

Figure labels "PECS" represent PECS2 open-path data, "PECS CP" represent PECS2 enclosed-path data, "in situ" represent the originally provided data while "TON LI75" represent *in situ* 10 Hz data independently processed values/data by the AmeriFlux Tech team using EddyPro ® (Version 5.2.1).

Turbulent fluxes[1]:

Turbulent fluxes (Figure 2 - Figure 8) calculated from the PECS2 and *in situ* sensors exhibited a reasonably good agreement. The CO_2 fluxes estimated with the open-path analyzers (Figure 2, slope: 0.81, offset: -0.28 µmol m^{-2} s^{-1}, R^2 = 0.97) diverted by 19% caused by the cumulated difference in data processing, CO_2 variance (please see section on IRGA scalars and statistics) and the rotated vertical wind

[1] Estimates of random flux uncertainties for the PECS2 turbulent fluxes accompany each figure. Uncertainty estimates were calculated following Finkelstein and Sims (2001) due to the ease of implementation and lack of parameters (see Billesbach, 2011 for a comparison of other methods).

component (please see Figure 27) and the consequently calculated covariance of vertical wind and CO_2 (Figure 3, slope: 0.55, offset: +0.00 µmol m^{-2} s^{-1}, R^2 = 0.96). The independently calculated *in situ* covariances agree better (Figure 3, slope: 0.93, offset: +0.00 µmol m^{-2} s^{-1}, R^2 = 0.99), indicating a difference in applied data processing method or quality check setting. A closer look at the comparison of the covariances and final CO_2 fluxes (see Figure 4) show the *in situ* covariance to be of a factor of a thousand's of the final fluxes (or vice versa) at different scale. Please investigate these variables and the steps carried out from covariance to final flux and the applied WPL term.

Latent heat fluxes agreed well with the *in situ* differing by 3 % from the PECS2 system (Figure 5, slope: 0.97, offset: -0.32 W m^{-2}, R^2 = 0.99) with the occasional scatter of more than ± 20 W m^{-2}. These differences were also mirrored in the covariance of vertical wind and water vapor (Figure 6, slope: 1.08, offset: -0.03 W m^{-2}, R^2 = 0.99), possibly caused by the difference in H_2O variance (please see section on IRGA scalars and statistics) and the rotated vertical wind component (see Figure 27).

Sensible heat fluxes showed a good agreement with a 7% difference (Figure 7, slope: 0.93, offset: -0.21 W m^{-2}, R^2 = 0.98) with an occasional scatter of more than ± 20 W m^{-2}. The independently processed values agree much better, showing a much better alignment along the ideal 1:1 line with only 2% difference. Friction velocity values showed a good agreement but with a frequent diversion of approximately 10% (in absolute terms) from the PECS2 system but with an overall deviation of 3% from the PECS2 sonic anemometer data (Figure 8, slope: 0.97, offset: -0.01 m s^{-1}, R^2 = 0.97). No shading by the PECS2 system on the tower to the North of the *in situ* eddy flux suite is apparent in Figure 9 with lowest friction velocity values originating from East and South-East.

To place the results in the context of the broader AmeriFlux network, we selected the gas and energy fluxes to benchmark (Figure 10) against the accumulated record of AmeriFlux site visits since 2002 (Schmidt *et al.*, 2012). To accomplish this, we changed the reference value from a site maximum (equation 1, see Schmidt *et al.*, 2012) to a fixed value (see Figure 10). The resulting relative instrumental error (*sensu* Schmidt *et al.,* 2012 and Figure 10 (current report)) represents the combined error originating from systematic (site dependent; instrumental, etc.) and random (combined site and PECS2; instrumental noise, change in ambient/environmental conditions, etc.) errors.

RIE values for variables derived from a single instrument requiring little additional corrections are usually smaller than amalgamated variables, such as final corrected fluxes, for example.

The ensemble averaged (co-)spectra from independently processed data for relevant terms recorded with the open-path systems are provided in Figure 11 and Figure 12, respectively. The spectra (Figure 11) of the sonic components correspond rather well but it appears the *in situ* sonic anemometer to tail off slightly in the high frequency domain. This could be attributed to signal aliasing which would be consistent since aliasing may affect the spectra and co-spectra but should not affect the end fluxes or variance *per se (*Massman*,* 2000) (Figure 11). The co-spectra estimated from both open-path systems agreed very well.

IRGA scalars and statistics:

The overall CO_2 mole densities (Figure 13, slope 0.94, offset: +0.80 mmol m^{-3}, R^2 = 0.99) recorded with the open-path gas analyzers agreed rather well. There is an obvious pattern in the difference (middle panel, Figure 13), that reappears regularly each day. A comparison between the two PECS2 systems shows this pattern to reappear in a slightly different manner (see middle panel Figure 15) indicating that the repetitive peak in Figure 13 (middle panel) is possibly caused by temporary insolation of the PECS2 LI-7500A temperature probe early afternoon (Figure 14).

In situ staff also provided CO_2 concentrations as mixing ratio. These are 20% lower than those estimated from the PECS2 open-path gas analyzer at times while the difference in density is only 7%. Comparing available mixing ratios from *in situ* data with those estimated using EddyPro from independently processed *in situ* data together with enclosed-path analyzer data we observe large discrepancies between provided mixing ratios and those estimated by the AmeriFlux Tech team (Figure 15 and Figure 16). Figure 16 highlights those time periods when the *in situ* air temperature was diverting by more than 1°C (please also see Figure 34 and Figure 36) from the PECS2 aspirated R.M. Young probe. As a reference we have also added those concentration values estimated independently from the *in situ* raw data. Note that the AmeriFlux Tech team provides calibration gases (check and span) at no cost to active AmeriFlux sites to conduct their own calibrations or calibration checks.

The variance of CO_2 (Figure 17, slope 0.75, offset: -0.00 (mmol m^{-3})^2, R^2 = 0.95), showed a difference of 25% when comparing the two open-path systems. Adding the independently calculated variances from raw *in situ* data we find this high discrepancy between these and PECS2 to disappear (Figure 17, slope: 0.95, offset: +0.00 (mmol m^{-3})^2, R^2 = 0.99). The independently processed *in situ* data were processes by applying the same corrections, filtering and QC attributes as has been applied to the PECS2 open-path data.

The water vapor mole density recorded with the *in situ* and PECS2 open-path gas analyzers showed a clear offset (Figure 18, slope: 1.03, offset: +39.73 mmol m^{-3}, R^2 = 0.98) of approximately 50 mmol m^{-3} in one of the two gas analyzers. Comparing the PECS2 open-path with the PECS2 enclosed-path analyzer values (Figure 19, slope: 1.02, offset: +1.72 mmol m^{-3}, R^2 = 0.99) it becomes apparent that the offset is recorded with the *in situ* gas analyzer (please also see Figure 37). Comparing the variances between the two open-path gas analyzers, they show a discrepancy of 15% (Figure 20, slope: 1.15, offset: 3.79 (mmol m^{-3})$^{-2}$, R^2 = 1.00). Independently estimated values show only a 4% improvement when comparing *in situ* with PECS2 data. We recommend regular calibration checks and calibrations of gas analyzers to be carried out in lab conditions. As already briefly mentioned, the AmeriFlux Tech team provides calibration gases (check and span) at no cost to active AmeriFlux sites.

Sonic wind components and temperature:

Wind direction values showed a distinctive diurnal pattern throughout the measurement period. The wind direction estimated with the *in situ* sonic anemometer (Gill-Windmaster Pro) deviated by several degrees when comparing with the PECS2 sonic anemometer (Gill R3-50) (Figure 21, slope: 1.02, offset: -41.59°, R^2 = 1.00). The AmeriFlux Tech team measured locations, heights and orientation of all PECS2 and *in situ* instruments (Appendix 1). Using this information, we independently estimated the wind direction from *in situ* raw data and found much closer agreement (Figure 21, slope: 1.01, offset: +11.21°, R^2 = 1.00). Please verify orientation of the *in situ* sonic anemometer. The mean horizontal wind speed comparison from the sonic anemometers was excellent (Figure 22, slope: 1.01, offset: +0.02 m s^{-1}, R^2 = 1.00). Figure 23 and Figure 24 show the distinctive wind distribution for daytime (Figure 23) and nighttime (Figure 24) estimated from PECS2 data.

Differences of up to 11% were observed in the variances of rotated wind components (Figure 25 - Figure 27) with the rotated vertical-wind w-component being 11% higher than the PECS2 values (Figure 27, slope: 0.89, offset: +0.00 m s^{-1}, R2 = 0.99), while the horizontal u-component and cross-wind v-component showed 1-2% variation, respectively (Figure 25, slope: 1.01, offset: +0.02 m s^{-1}, R^2 = 0.99 and Figure 26, slope: 0.98, offset: +0.02 m s^{-1}, R^2 = 0.99). Exceptionally high winds on 15th April appear to have caused 6% of the visible difference (see Figure 28).

Figure 29 illustrates the averaged footprint distribution estimated from PECS2 data for the entire site visit duration using the Kormann and Meixner (2001) model. The additional Figure 30 has been included to show the distinctive diurnal changes in atmospheric stability that can change the footprint size (90% distance) over the course of the day (nighttime range extends beyond 5km at times) and the distribution of the maximum source location throughout the visit duration.

From our experience the Gill R3-50 (used on the PECS2) does not measure absolute sonic temperature very well. That said, the sonic anemometer followed the temperature relatively well (Figure 31, slope: 0.76, offset: +1.91^{o}C, R^2 = 0.98) with highest discrepancies during daytime hours on sunny days. There is a minimal difference between *in situ* and independently processed raw *in situ* data, pointing to a different processing method. The variance in recorded sonic temperature (Figure 32, slope: 0.84, offset: +0.01^{o}C, R^2 = 0.88) showed some scatter and a discrepancy of 16 % likely to contribute to the deviating sensible heat fluxes (Figure 7). Again, divergences in data are probably due to differences in data treatment. In order to investigate the performance of the *in situ* sonic anemometer (Gill Windmaster Pro) we also include the comparison of both sonic temperature values, converted to true temperature, with the *in situ* and PECS2 ambient air temperature readings (Figure 33). Included is also the comparison between both PECS2 ambient air temperature measurements: HMP155 and the aspirated RM Young probe (Figure 33, right panel).

Meteorological and radiation measurements:

Air temperature measurements reported by the PECS2 Vaisala HMP155 and *in situ* Vaisala HMP45 sensors tracked closely to some degree (Figure 34, slope: 1.06, offset: -2.31 ^{o}C, R^2 = 0.84) with similar values during daytime hours but with divergences of higher than 5 ^{o}C during some nights. In order to identify which of the two air temperature probes appears misreporting true values we point to the right panel in Figure 33. This shows the excellent agreement between the two temperature probes that are part of the PECS2 instrument suite. These are being factory calibrated at the beginning of each year. Furthermore, a malfunctioning of the in situ HMP probe does mirror in the relative humidity readings (Figure 35, slope: 0.89, offset: +12.73 %, R^2 = 0.73) leading to a discrepancy of over 20 % in absolute terms. Included Figure 36 illustrates the discrepancies in air temperature and relative humidity, showing all respective data together with those values with a discrepancy of less than 2°C.

Illustrating relative humidity values estimated from all gas analyzers in Figure 37 supports the hypothesis of a malfunctioning *in situ* probe. We recommend investigating this by adding comparisons with other temperature and relative humidity measurements carried out at the site and the probe being sent for service and factory calibration (both, temperature and relative humidity). Using these nighttime values of air temperature and relative humidity readings lead to erroneous estimation of site important properties, such as evapotranspiration, respiration, stability (via sensible heat flux coeff.) and storage, for example. And as already demonstrated, gas mixing ratio conversions. The atmospheric pressure measurements tracked closely (Figure 38, slope: 0.97, offset: +2.27 kPa, R^2 = 0.98).

The incoming shortwave radiation from the *in situ* CNR1 radiometer traced the PECS2 incoming radiation very well (Figure 38, slope: 1.00, offset: +1.39 W m^{-2}, R^2 = 1.00). The pattern in the middle panel is a sign of a slight levelling issue of one of the two radiation booms. The apparent gaps during night-time hours are gaps in the *in situ* data. This appears to be caused by a data acquisition setting that eliminates negative values at night. Please revisit the settings and investigate the real night time values. The outgoing shortwave radiation (Figure 40, slope: 1.01, offset: +0.34 Wm^{-2}, R^2 = 1.00) agreed well during night time hours with deviations of up to 5 Wm^{-2} from the *in situ* radiometer during daytime hours with an overall diversion of 1% from the PECS2 measurements.

Incoming longwave radiation (Figure 41, slope: 1.10, offset: -34.83 W m^{-2}, R^2 = 0.95) recorded with the *in situ* radiometer showed differences of 10% compared to the PECS2 system. This translated into differences of ± 10 Wm^{-2} with outgoing longwave radiation (Figure 42, slope: 0.99, offset: +9.03 W m^{-2}, R^2 = 0.98) showing a much smaller difference in the comparison. The different outgoing longwave radiation values can also result from the different field of view of the two radiometers recording different surface covers. Each of the longwave radiation components includes a temperature term in their calculation which, when used individually can differ from the true longwave radiation but cancels out when estimating the net value. The internal temperature probe can only give accurate readings when in thermal equilibrium, which in a malfunctioning state can lead to individual long wave radiation readings to divert by several Wm^{-2} from the true value. That said, the comparison between the CNR1 and the PECS2 CNR4 body temperatures (Figure 43, slope: 0.98, offset: +1.57°C, R^2 = 1.00) show a discrepancy of only 2 % which translates into a deviation of over 2°C at times, roughly 12 Wm^{-2} in energy terms.

The net radiation comparison between the PECS2 CNR4 and the *in situ* NRLite Net radiometer went well (Figure 44, slope: 0.99, offset: +1.55 W m^{-2}, R^2 = 1.00) with a slight deviation of more than 50 W m^{-2}. That said a closer look at the middle panel shows a distinctive pattern in the comparison between these two instruments during late mornings. This very abrupt change in difference lets suggest that it is caused by a change of instrument (PECS2) from shade to sun, possibly caused by the sun rising over the tree tops and hitting the PECS2 radiometer first. The *in situ* system exhibited a larger range compared to the PECS CNR4, resulting in higher values around solar noon translating into approximately 20 W m^{-2} lower net radiation values. The distinctive diurnal pattern observed in the middle panel in Figure 39 - Figure 47 is caused by the tilt of one of the radiation booms (Figure 45) causing the readings of each individual quantum, pyranometer and pyrgeometer sensor.

Incoming photosynthetic active radiation (PAR) from the *in situ* PAR quantum sensor showed a very good agreement with the PECS2 PQS1 (Kipp & Zonen) sensor (Figure 46, slope: 0.95, offset: -6.27 µmol m^{-2} s^{-1}, R^2 = 1.00) but with daytime readings underreporting those of the PECS2 sensor by over 100 µmol m^{-2} s^{-1}. Again, a distinctive pattern is being observed with a diurnal trend in radiation distribution, possibly caused by a slight tilt of one of the sensors together with a temporarily shading that is causing the double-peaked pattern.

A similar pattern is being observed in the reflected PAR readings (Figure 47, slope: 1.03, offset: +0.02 µmol m^{-2} s^{-1}, R^2 = 1.00) with the *in situ* probe possibly underreporting reflective values. Another plausible reason for the different readings could be the different field of view of the two down facing PAR quantum sensors. Note that the AmeriFlux Tech team provides calibrated PAR sensors at no costs to sites to conduct their own calibrations.

The *in situ* staff provided global and diffuse PAR values recorded with the Delta-T BF5 global and diffuse sunshine sensor. The PECS2 Delta-T SPN1 only measures shortwave radiation as total and diffuse. In order to include these measurements, we converted the SPN1 values to photosynthetic active radiation using a multiplier commonly used in the literature (Papaioannou *et al.*, 1993; Udo and Aro, 1999; Tsubo and Walker, 2005). For long time series this multiplier is not recommended as the ratio between PAR and broadband radiation is changing according to time of day and time of year (Jacovides *et al.,* 2004; Li *et al.*, 2010). Nevertheless, this short comparison went relatively well (Figure 48 and Figure 49). Values showed a difference of 3 – 8 % which are probably attributed to the conversion from broadband radiation (350 – 2700nm) to PAR (400 – 700nm) and instrument deterioration.

References:

Billesbach, D. P. (2011), Estimating uncertainties in individual eddy covariance flux measurements: A comparison of methods and a proposed new method, Agric. For. Meteorol. 151, 394–405, doi:10.1016/j.agrformet.2010.12.001.

Finkelstein, P. L., and P. F. Sims (2001), Sampling error in eddy correlation flux measurements, J. Geophys. Res., 106(D4), 3503–3509, doi:10.1029/2000JD900731.

Jacovides, C. P., Timvios, F. S., Papaioannou, G., Asimakopoulos, D. N., and Theofilou, C. M. (2004), Ratio of PAR to broadband solar radiation measured in Cyprus. Agricultural and Forest Meteorology, 121(3), 135-140.

Kormann, R., and Meixner, F. X. (2001), An analytical footprint model for non-neutral stratification. Boundary-Layer Meteorology, 99(2), 207-224.

Li, R., Zhao, L., Ding, Y., Wang, S., Ji, G., Xiao, Y., ... and Sun, L. (2010), Monthly ratios of PAR to global solar radiation measured at northern Tibetan Plateau, China. Solar Energy, 84(6), 964-973.

Massman, W.J. (2000), A simple method for estimating frequency response corrections for eddy covariance systems. Agric. For. Meteorol. 104.3: 185-198.

Nakai, T., Shimoyama, K., 2012. Ultrasonic anemometer angle of attack errors under turbulent conditions. Agric. For. Meteorol. 162–163, 14–26.

Nakai, T., van der Molen, M.K., Gash, J.H.C., Kodama, Y., 2006. Correction of sonic anemometer angle of attack errors. Agric. For. Meteorol. 136, 19–30.

Papaioannou, G., Papanikolaou, N., and Retalis, D. (1993), Relationships of photosynthetically active radiation and shortwave irradiance. Theoretical and Applied Climatology, 48(1), 23-27.

Schmidt, A., C. Hanson, W. S. Chan, and B. E. Law (2012), Empirical assessment of uncertainties of meteorological parameters and turbulent fluxes in the AmeriFlux network, J. Geophys. Res., 117, G04014, doi:10.1029/2012JG002100.

Tsubo, M., & Walker, S. (2005), Relationships between photosynthetically active radiation and clearness index at Bloemfontein, South Africa. Theoretical and Applied Climatology, 80(1), 17-25.

Udo, S. O., & Aro, T. O. (1999), Global PAR related to global solar radiation for central Nigeria. Agricultural and Forest Meteorology, 97(1), 21-31.

Table of Figures:

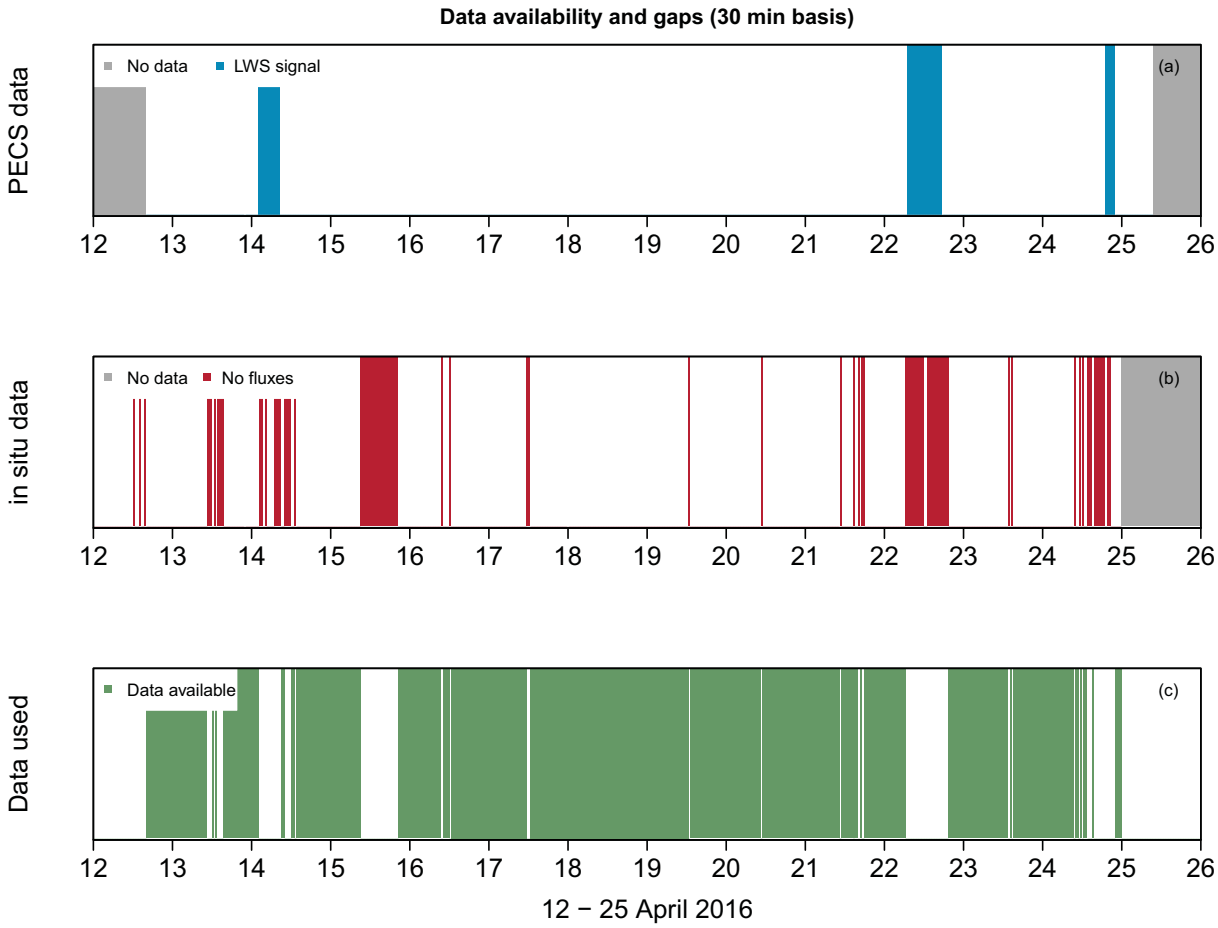

Figure 1 – Data availability for the PECS2 (panel a). Periods were flagged due to system outages or poor signal. "LWS" illustrates time when the leaf wetness sensor recorded wet periods, be it rain or dew. Data availability for the *in situ* system (panel b). As no *in situ* LI-7500 signal information is available, availability of CO_2 fluxes were used as a proxy. Summary of the data used for the inter-comparison are illustrated in panel (c).

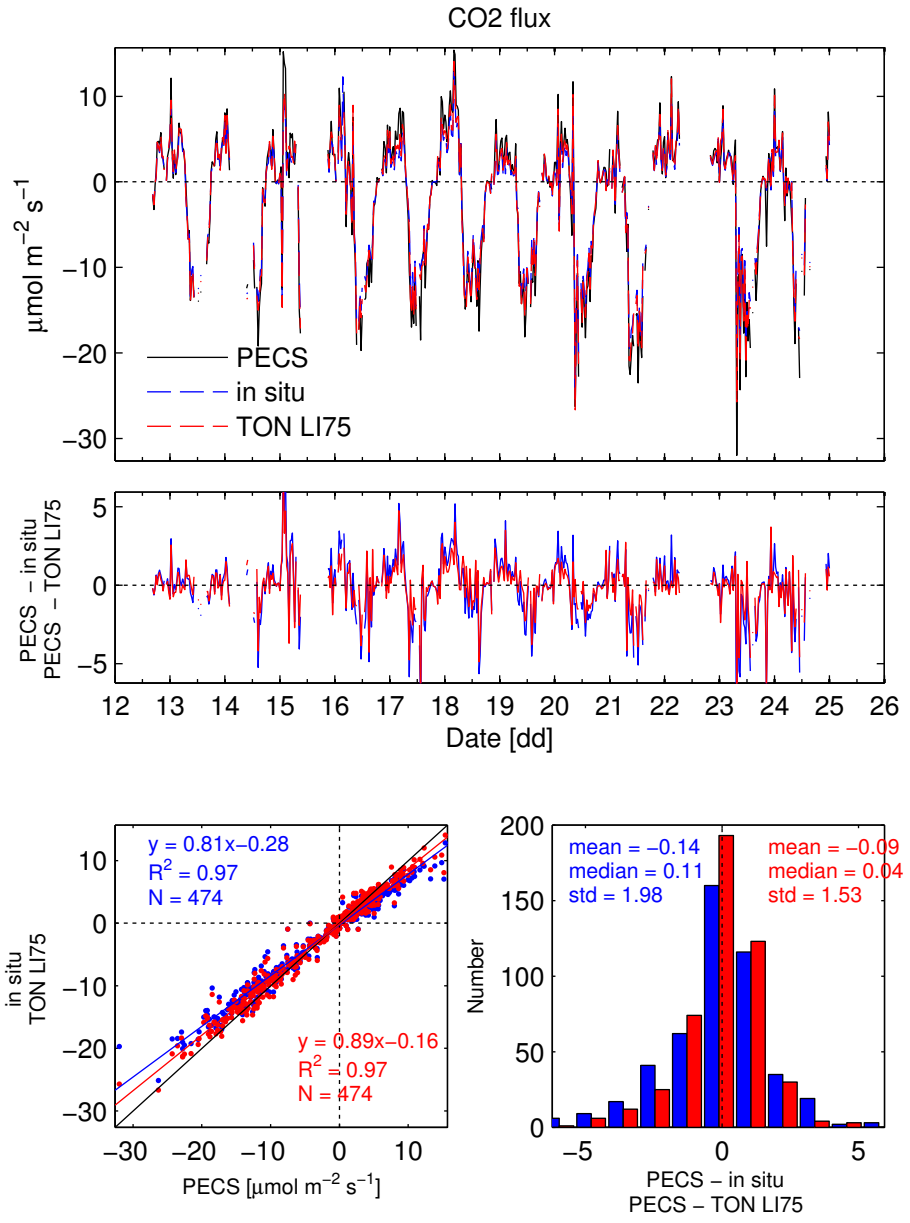

Figure 2 - CO_2 fluxes, estimated from open-path gas analyzers. ”PECS” represents PECS2 open-path data while “in situ” and “TON LI75” represent the *in situ* and the independently processed *in situ* data, respectively.

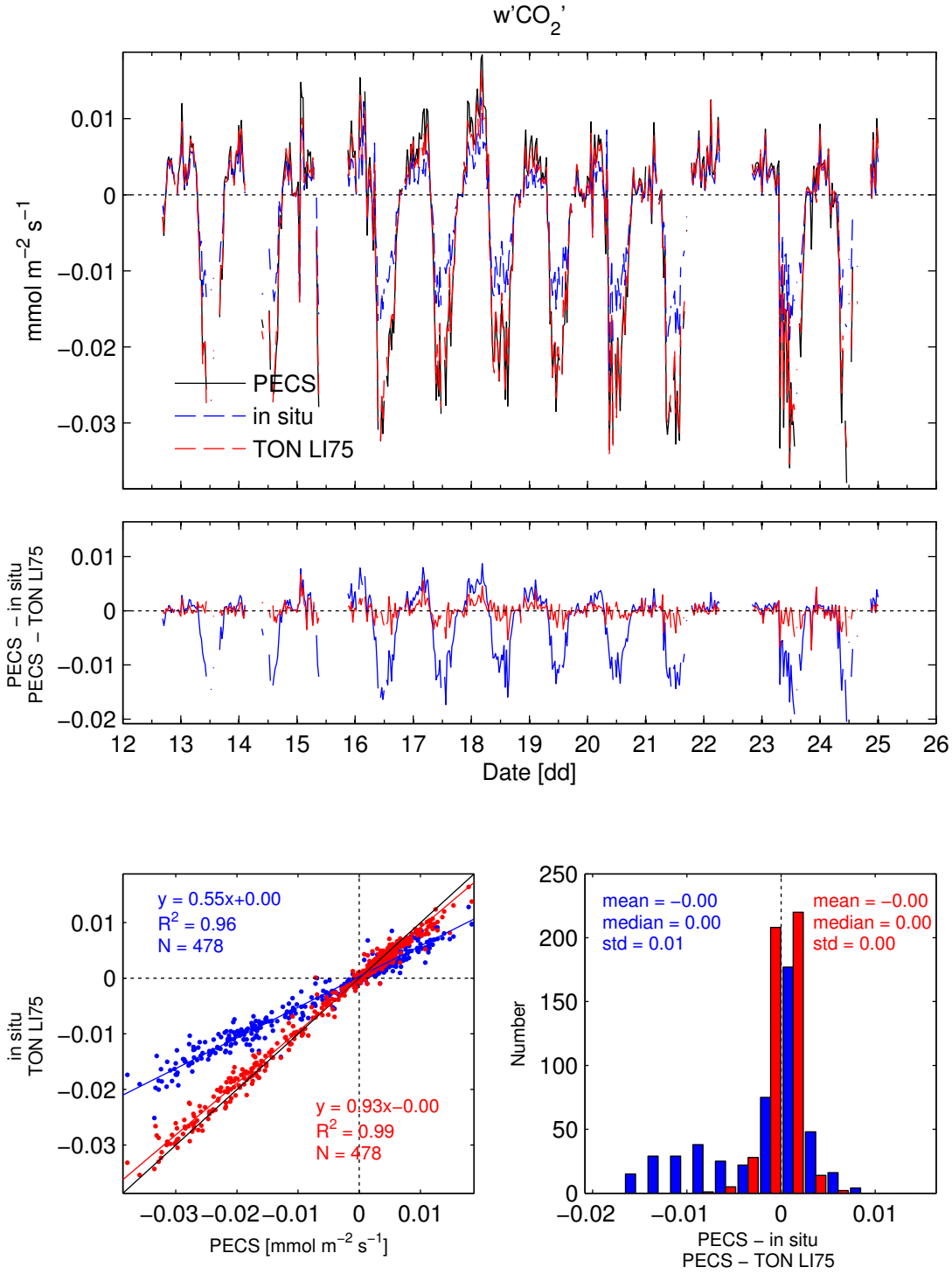

Figure 3 - Covariance of vertical wind and CO_2 measured with the open-path gas analyzers and the independently processed *in situ* (TON LI75) values.

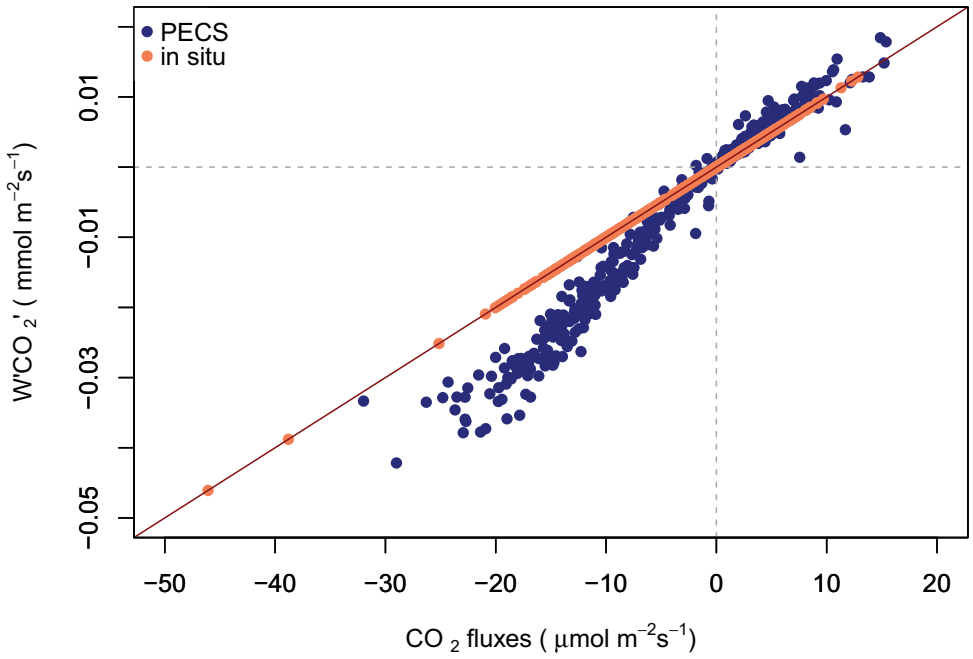

Figure 4 – Comparison of covariance of vertical wind and CO_2 and CO_2 fluxes for PECS and *in situ*.

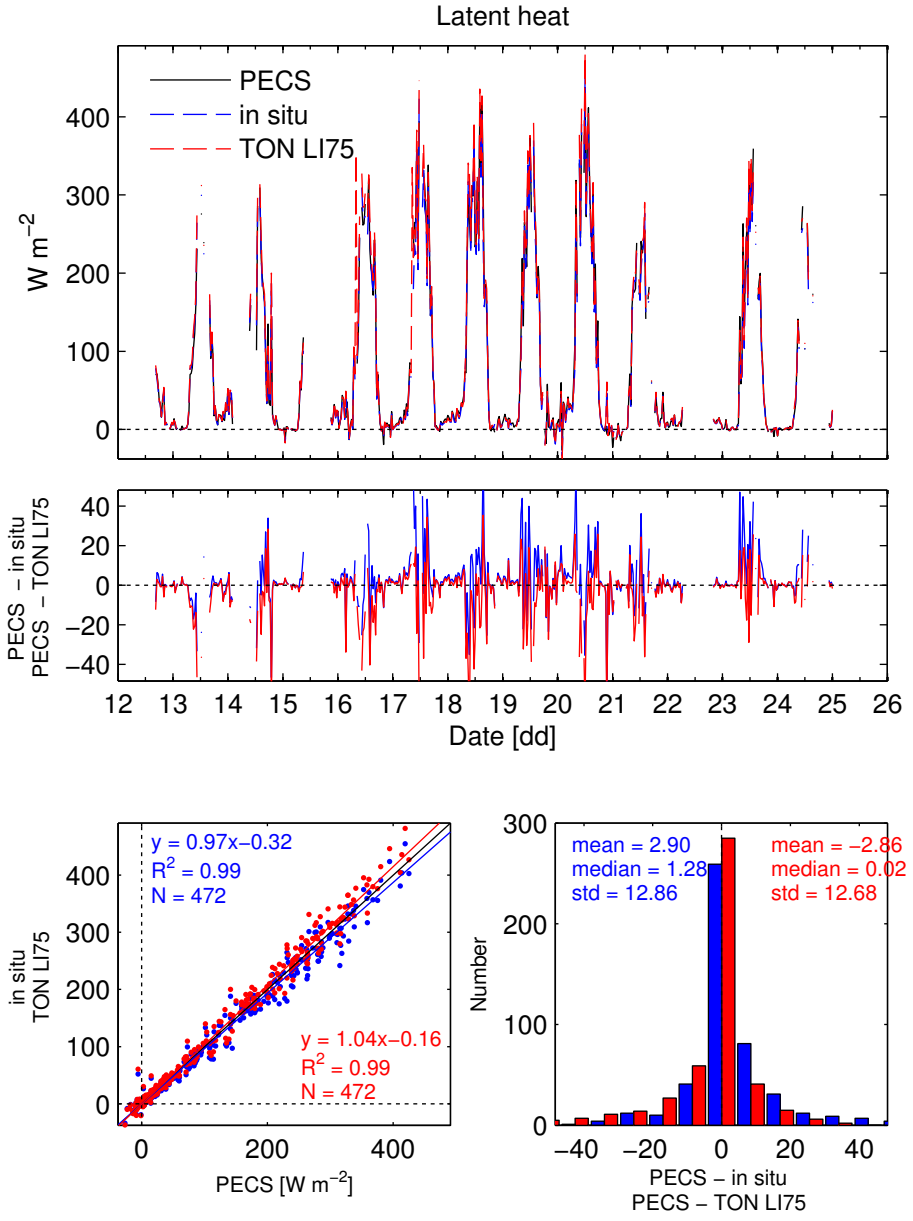

Figure 5 - Latent heat fluxes measured with the open-path gas analyzers. ”PECS” represents PECS2 open-path data while “in situ” and “TON LI75” represent the *in situ* and the independently processed *in situ* data, respectively.

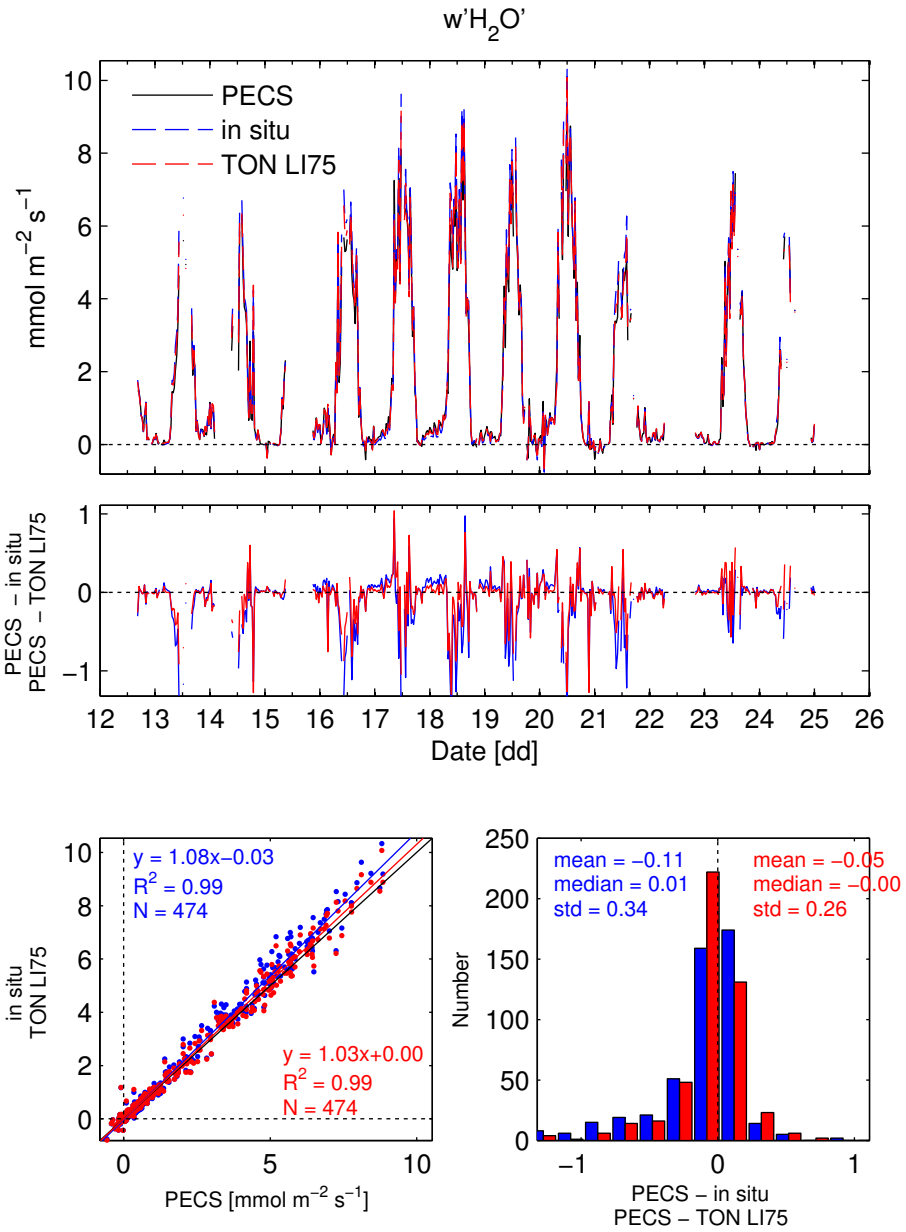

Figure 6 – Covariance of vertical wind and water vapor calculated from data recorded with the open-path systems. ”PECS” represents PECS2 open-path data while “in situ” and “TON LI75” represent the *in situ* and the independently processed *in situ* data, respectively.

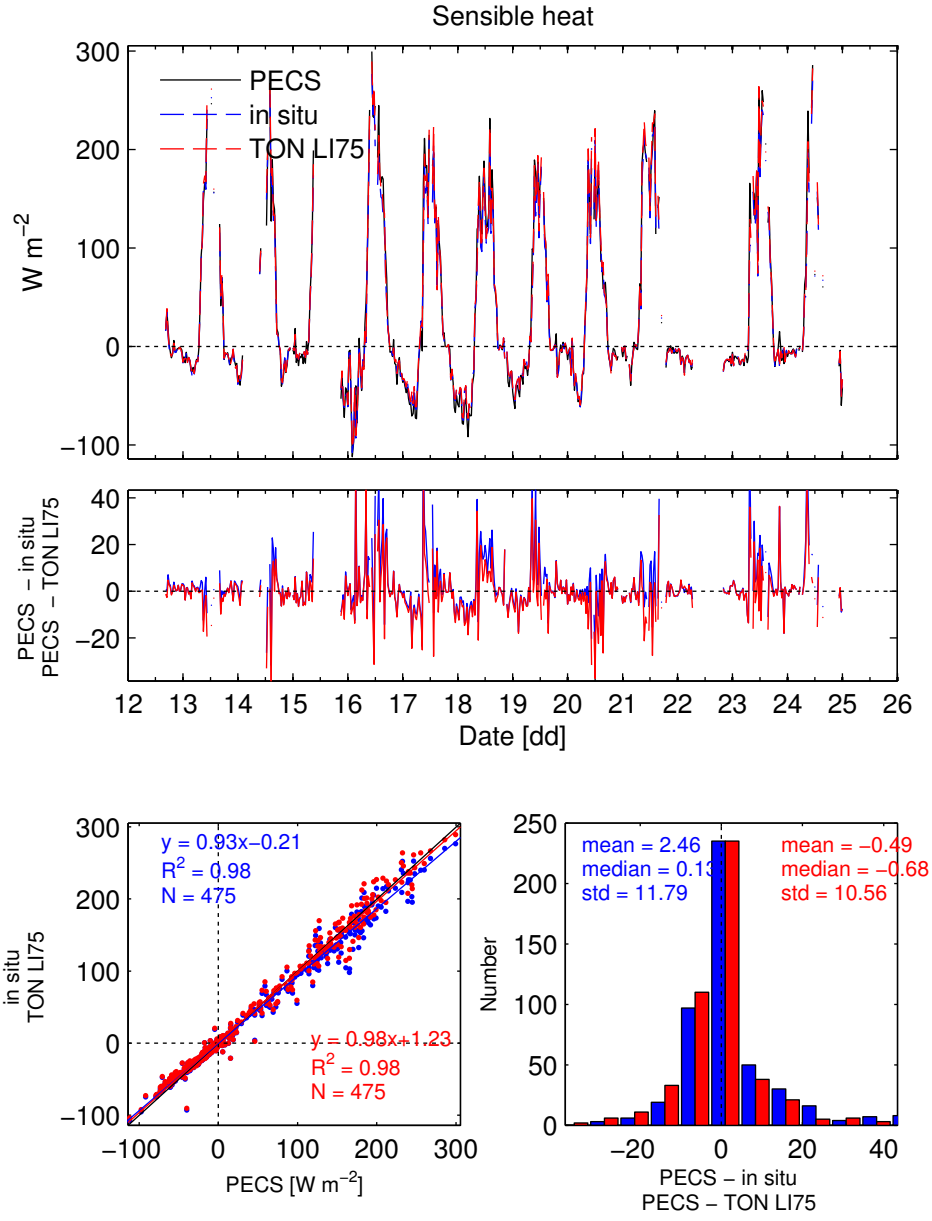

Figure 7 – Sensible heat flux. ”PECS” represents PECS2 open-path data while “in situ” and “TON LI75” represent the *in situ* and the independently processed *in situ* data, respectively.

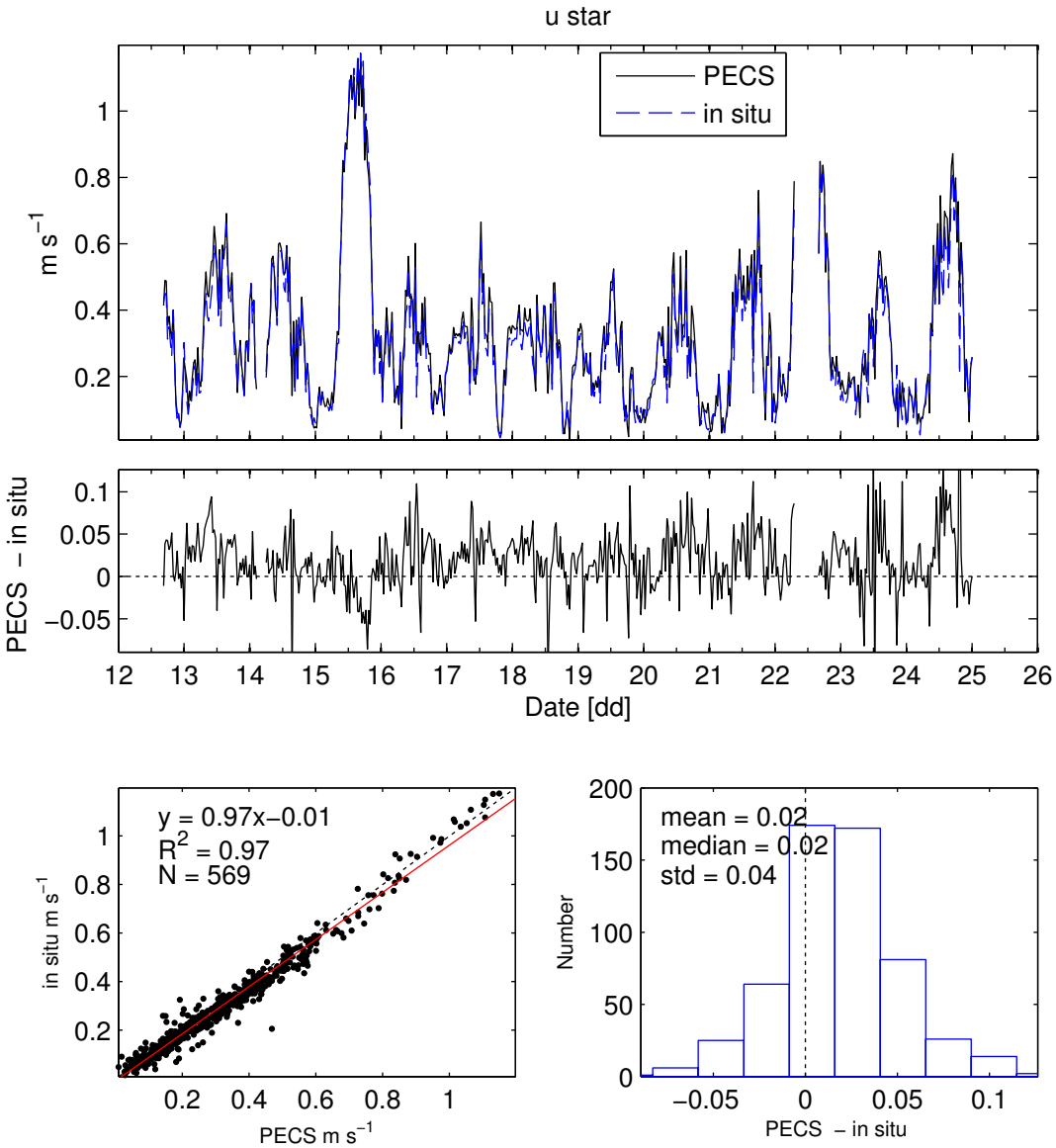

Figure 8 – Friction velocity.

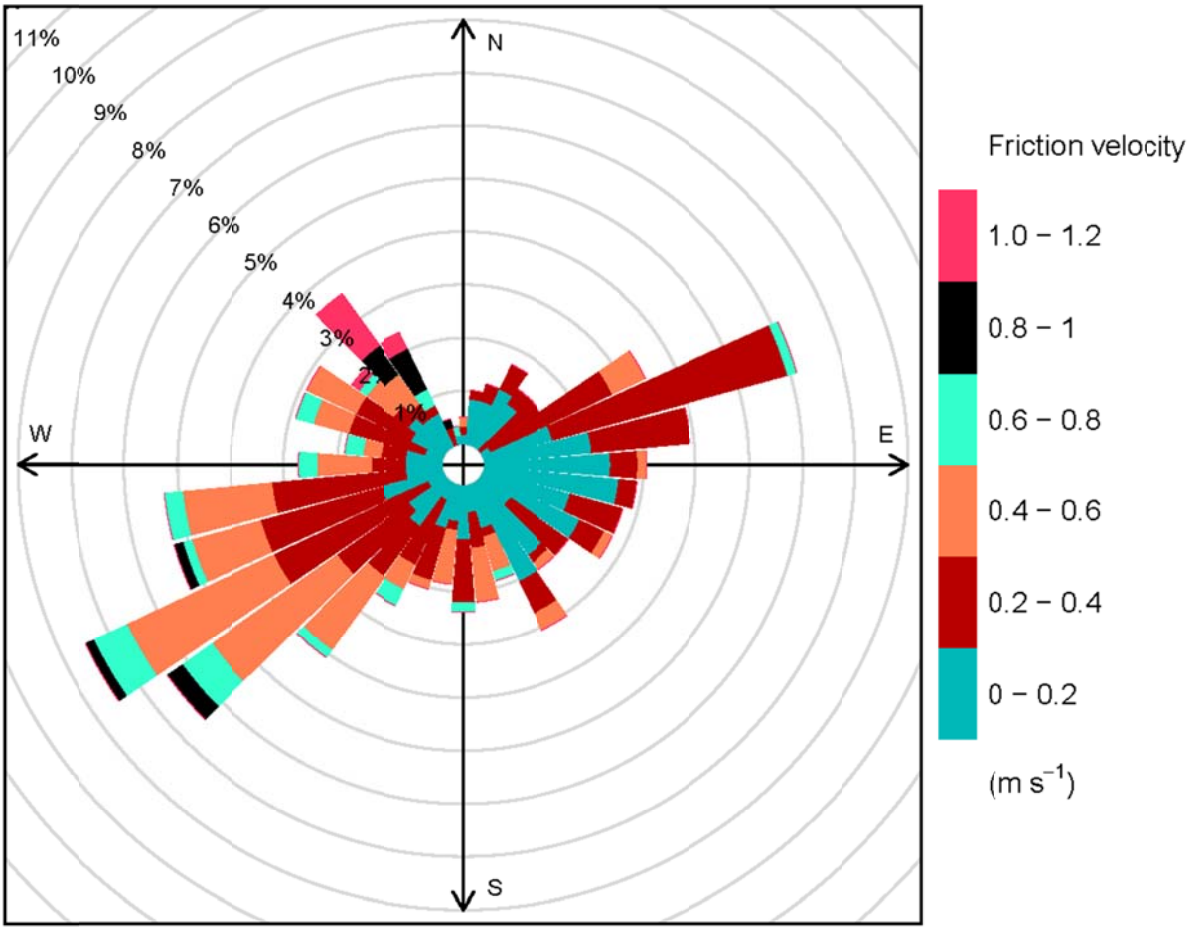

Figure 9 – Friction velocity according to wind direction calculated from PECS2 data.

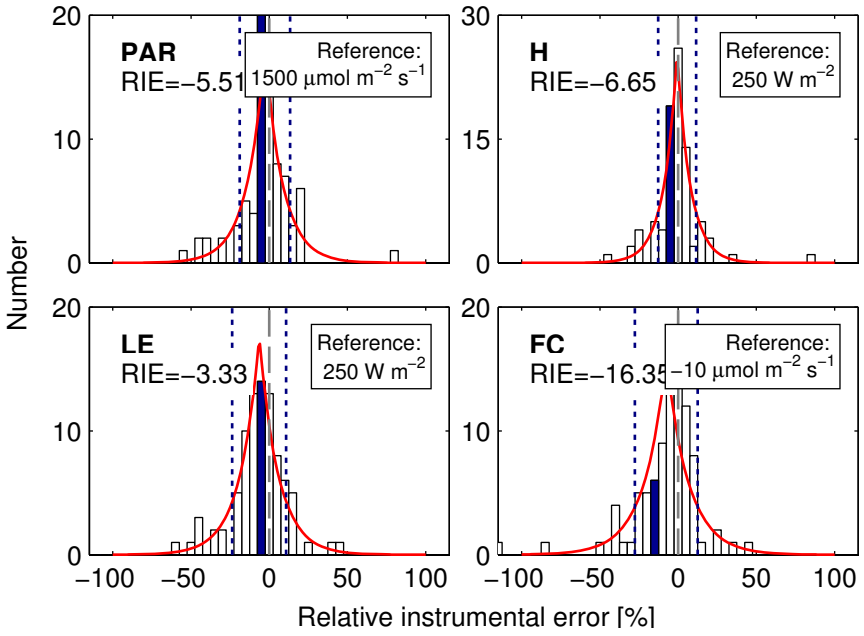

Figure 10 – Histogram of relative instrumental error (RIE) for 4 selected variables based on the accumulated record of AmeriFlux site visits. Colored bar denotes the RIE from this site visit (bar width = 5%). Laplace distribution illustrated in solid red line. Dashed, vertical lines denote mean ± √2β, where β is a scale parameter describing the Laplace distribution. The term √2β is equivalent to the standard deviation in a normal distribution. Negative RIE values indicate that on average the in situ system has recorded lower values than PECS2 (in this case) and vice versa.

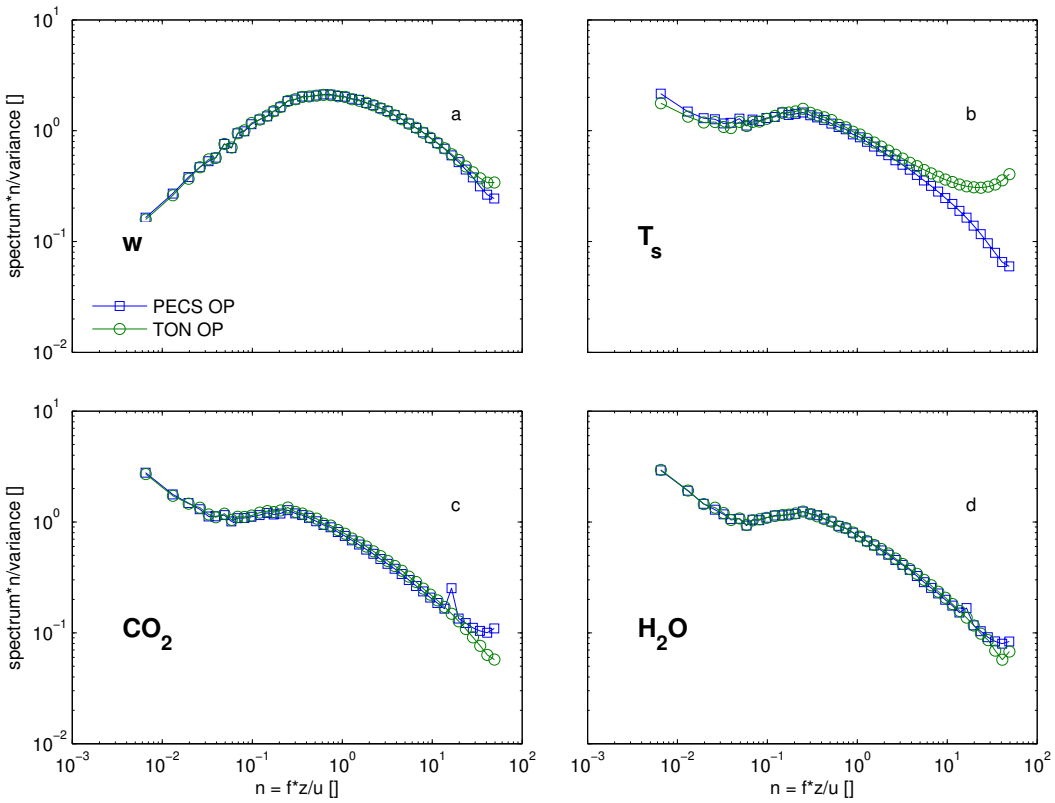

Figure 11 – Ensemble averaged spectra for the open-path systems.

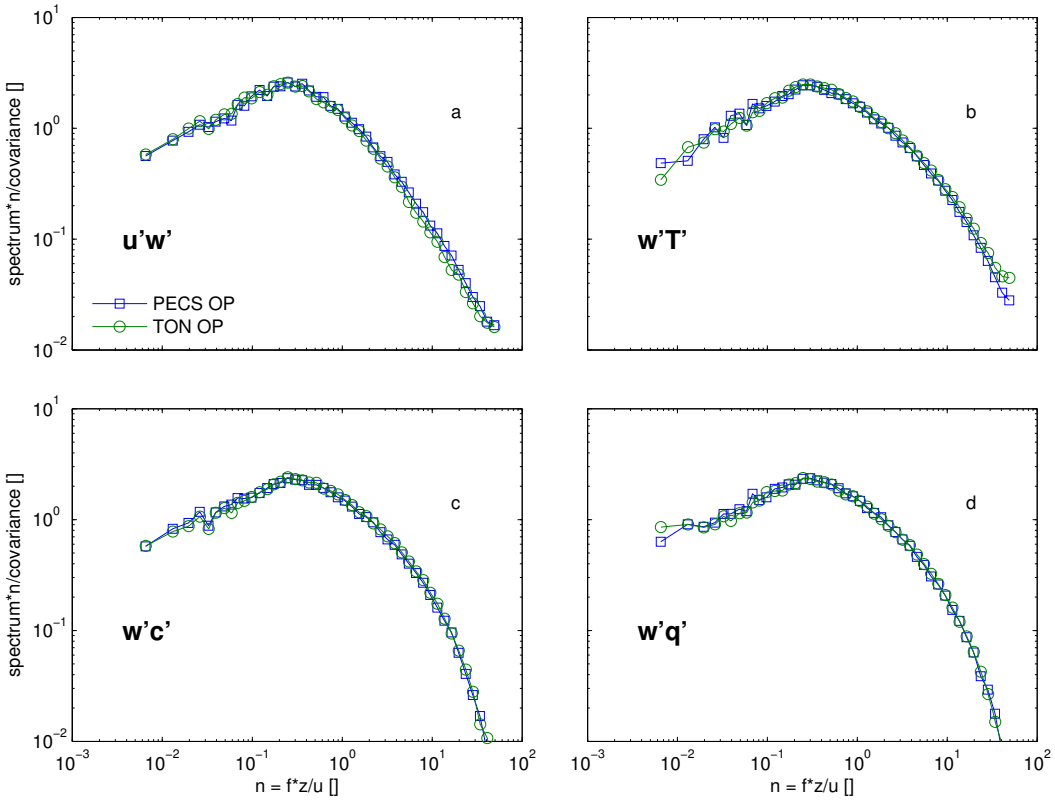

Figure 12 – Ensemble averaged co-spectra for the open-path systems.

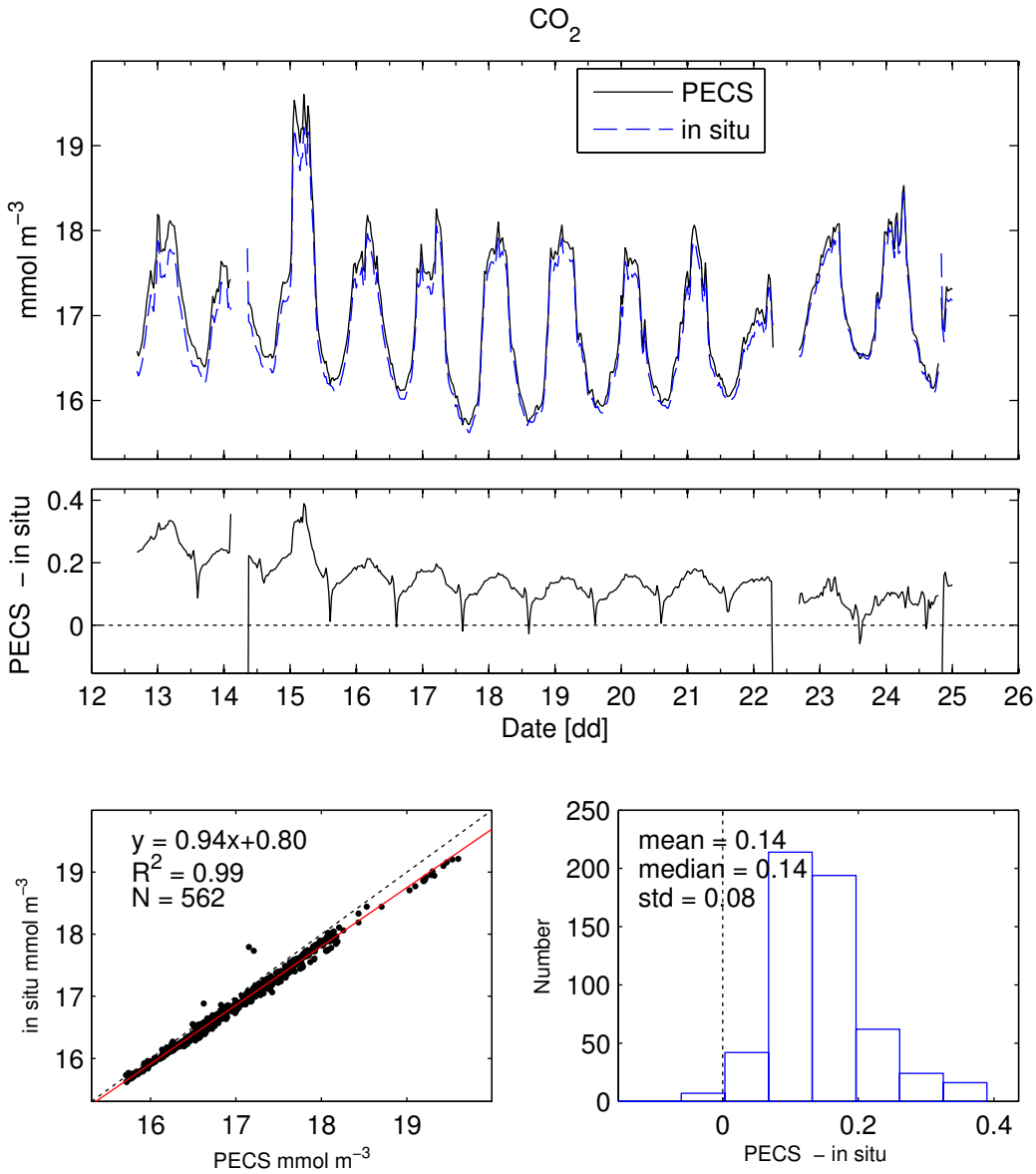

Figure 13 – CO_2 mole density recorded with the open-path gas analyzers.

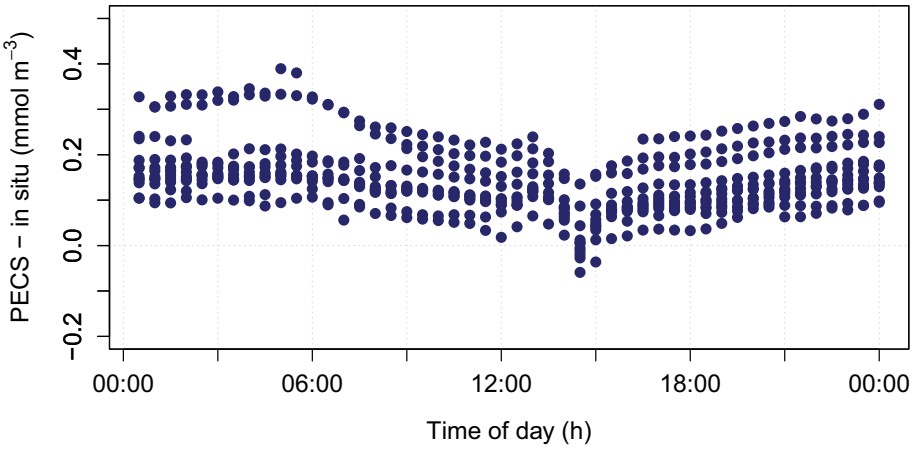

Figure 14 – Difference in CO_2 mole density by time of day.

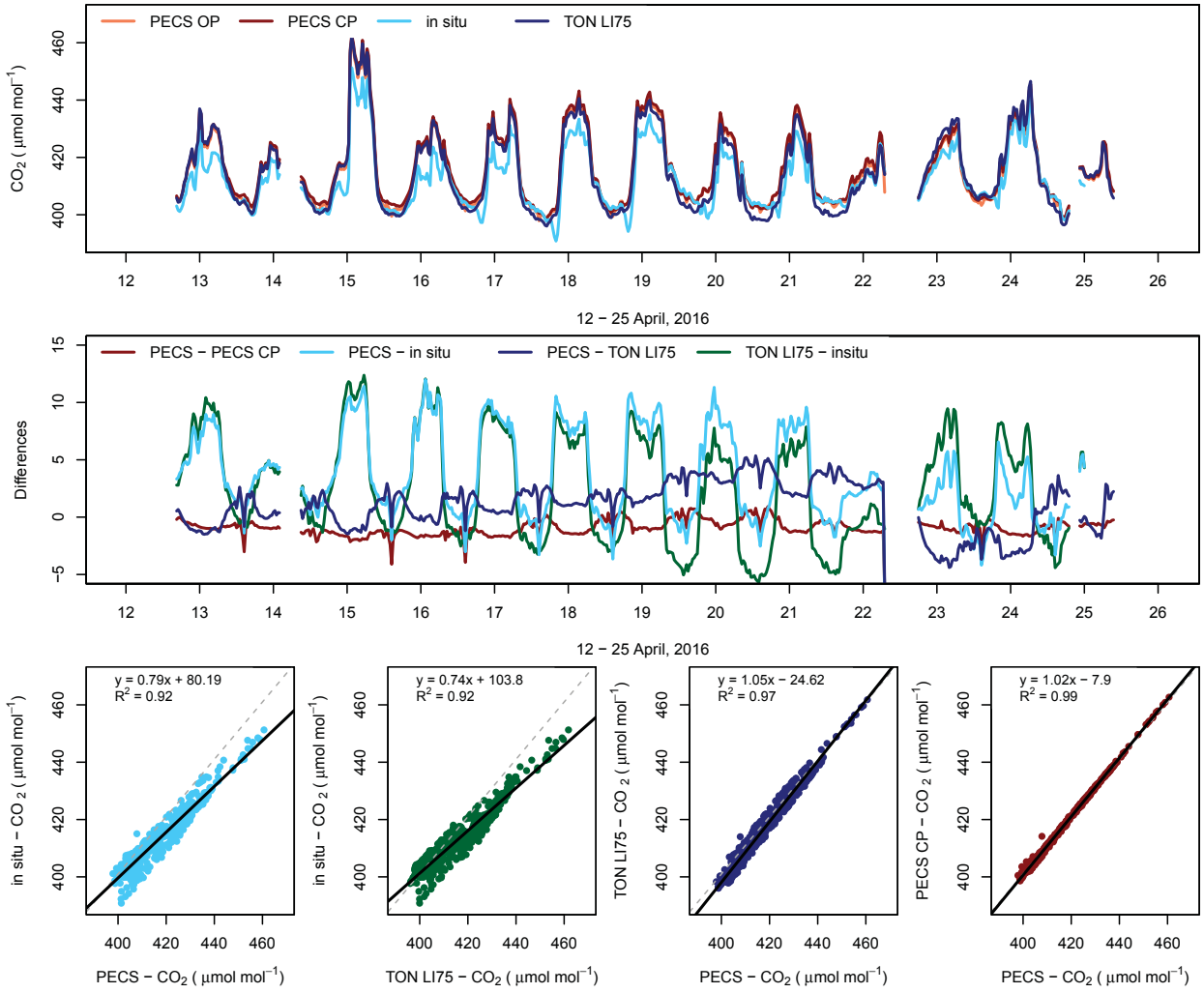

Figure 15 – CO_2 mixing ratio estimated from the open-path and enclosed gas analyzers. "in situ" illustrates the concentrations available from *in situ* data, "PECS" and TON LI75" mixing ratios estimated from the LI-7500s with EddyPro, while "PECS CP" those recorded with the PECS2 enclosed-path LI-7200.

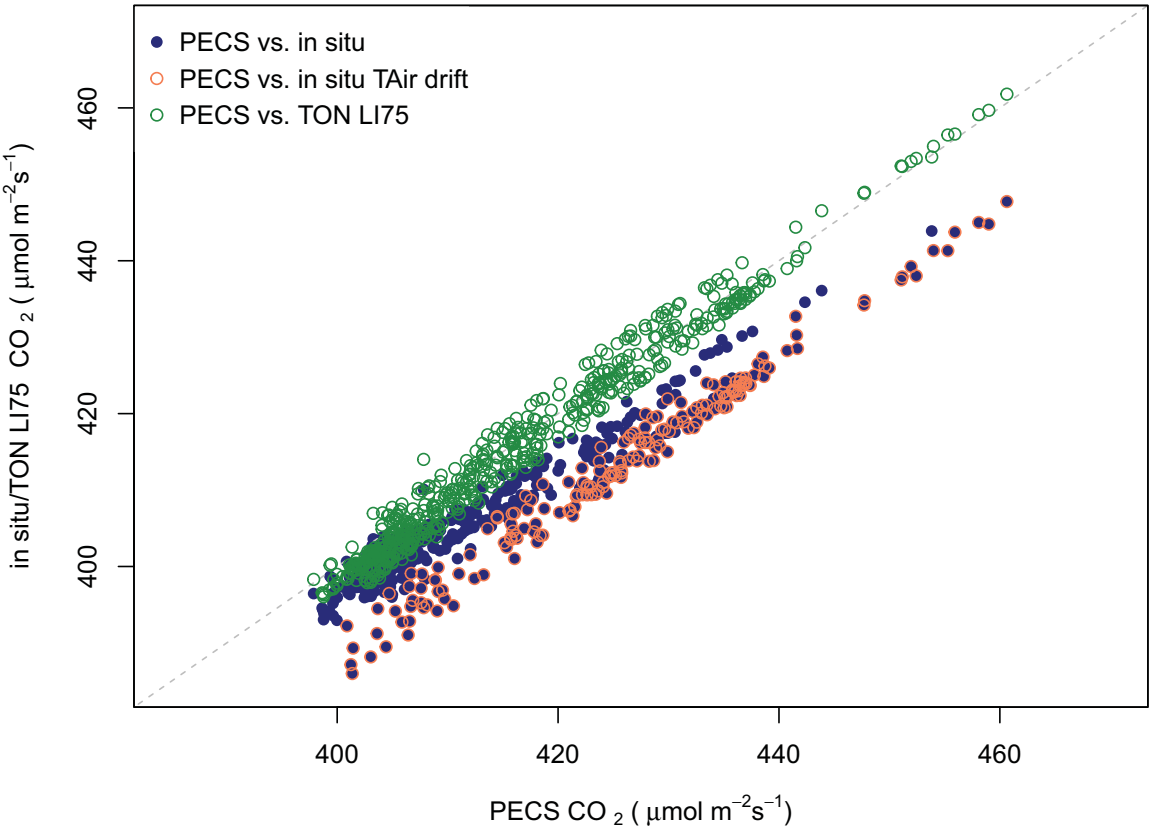

Figure 16 – Comparison of estimated CO_2 mixing ratio values estimated by the *in situ* staff, PECS open-path gas analyzer and from the independently *in situ* raw data. "in situ" illustrates the concentrations available from *in situ* data, "PECS" and TON LI75" mixing ratios estimated from the LI-7500s with EddyPro. "in situ TAir drift" highlight those data points for periods when the in situ ambient air probe diverged by more than 2 °C.

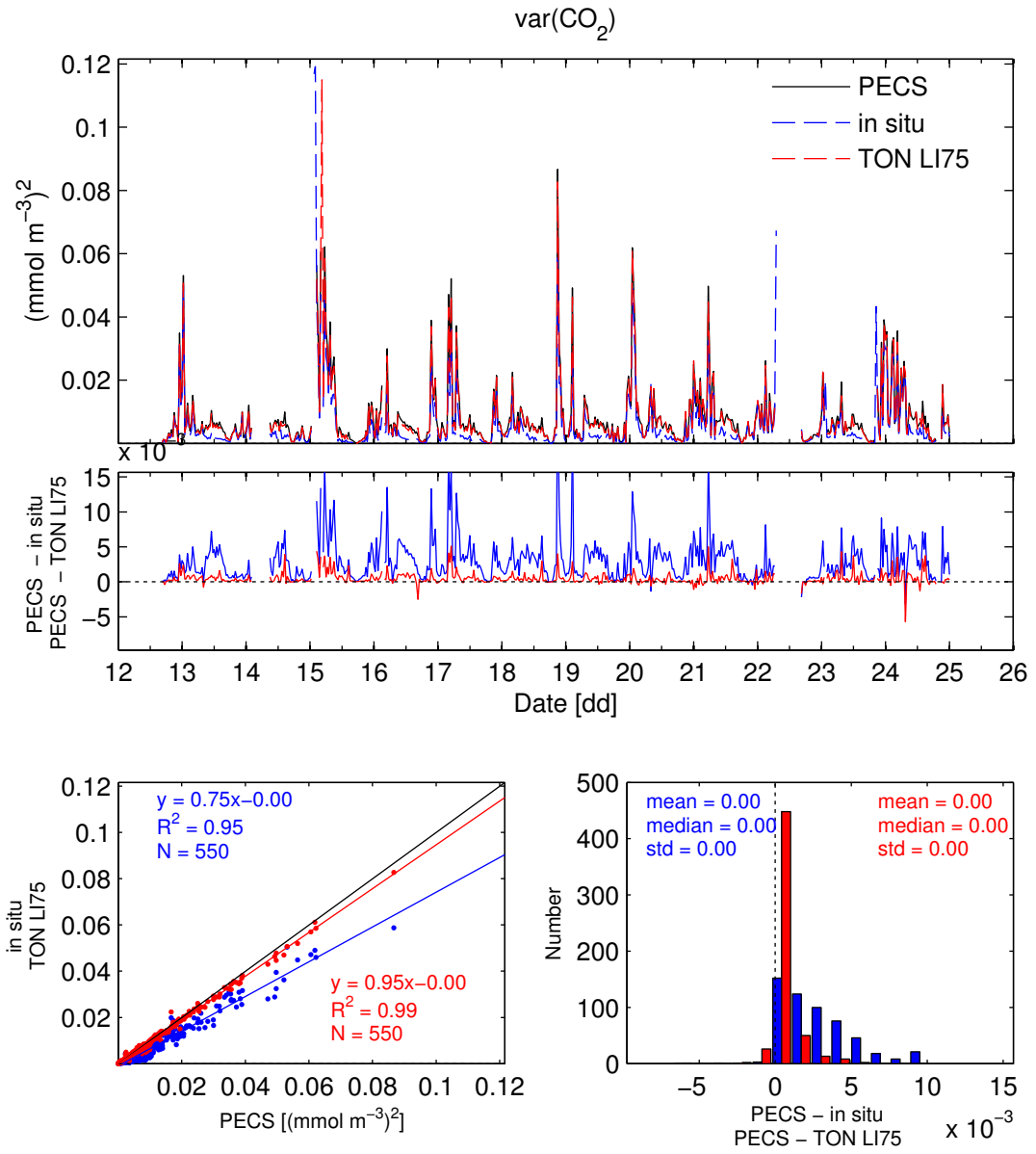

Figure 17 – Variance of carbon dioxide recorded with the *in situ* open-path gas analyzer, estimated by the *in situ* staff (in situ), independently estimated from *in situ* data by the AmeriFlux Tech team (TON LI75) and those originating from the PECS2 open-path gas analyzer (PECS).

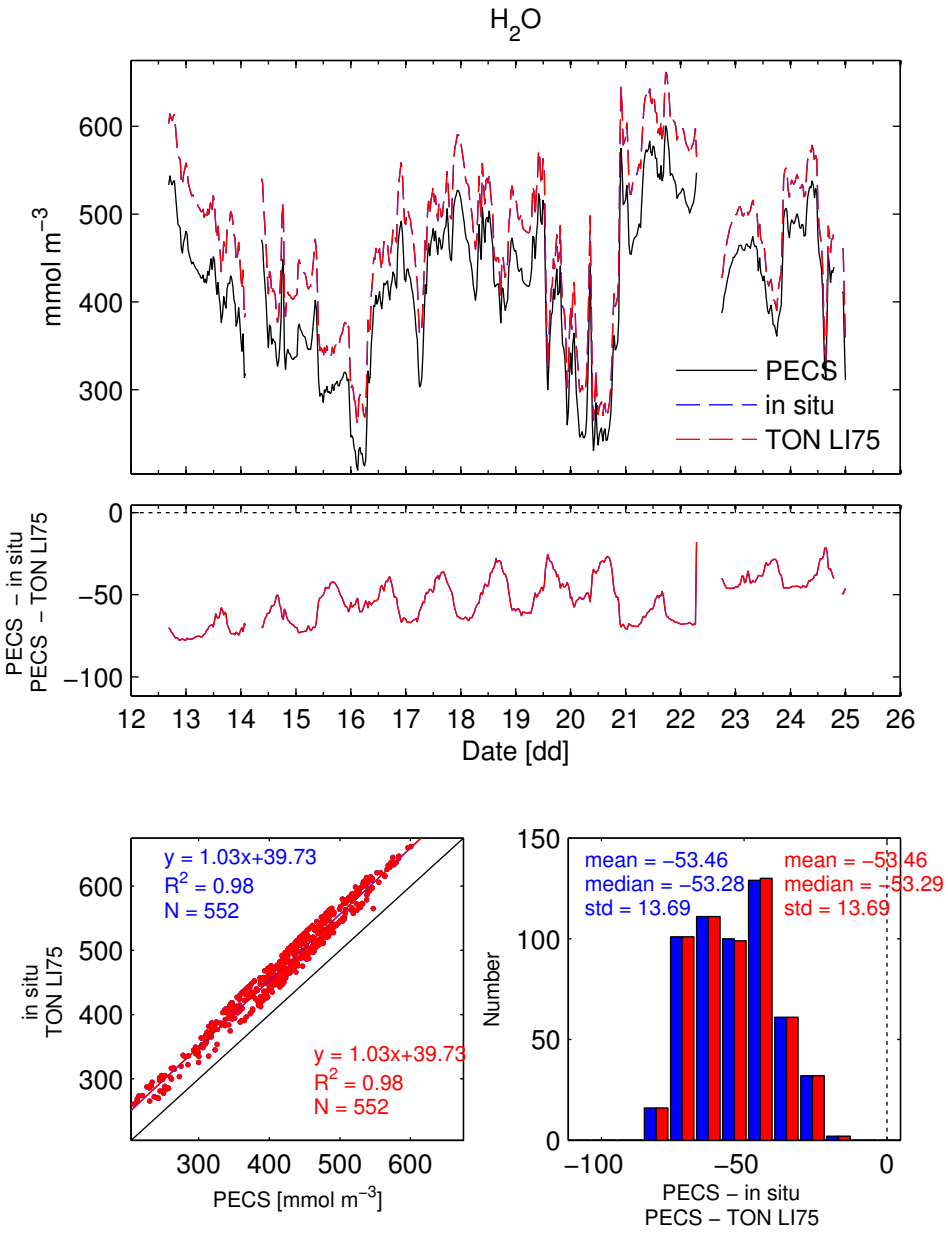

Figure 18 – Water vapor mole density recorded with the open-path gas analyzers.

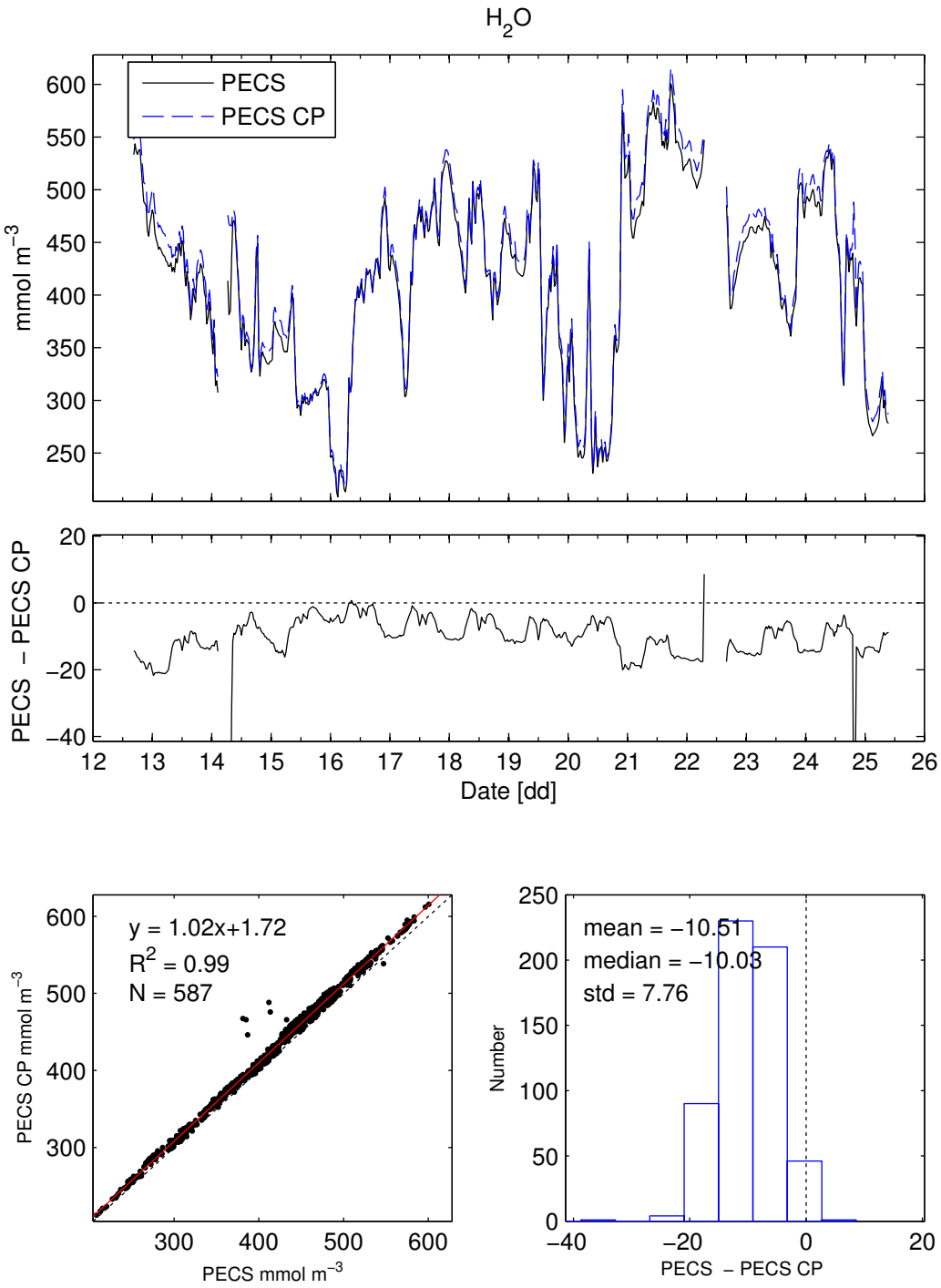

Figure 19 –Water vapor mole density recorded with both PECS2 gas analyzers: open-path (PECS) and enclosed-path (PECS CP).

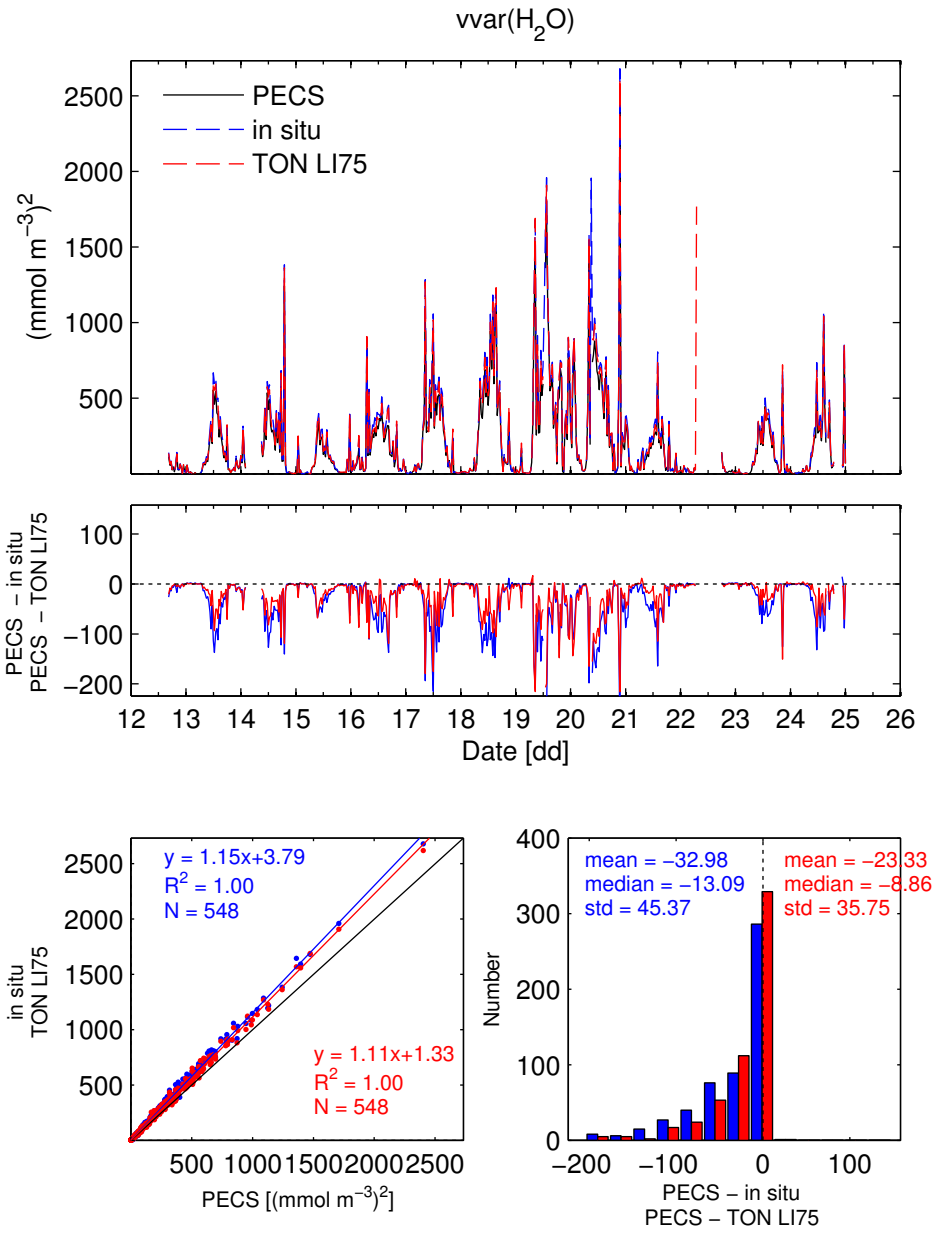

Figure 20 – Variance of water vapor mole density recorded with the open-path gas analyzers.

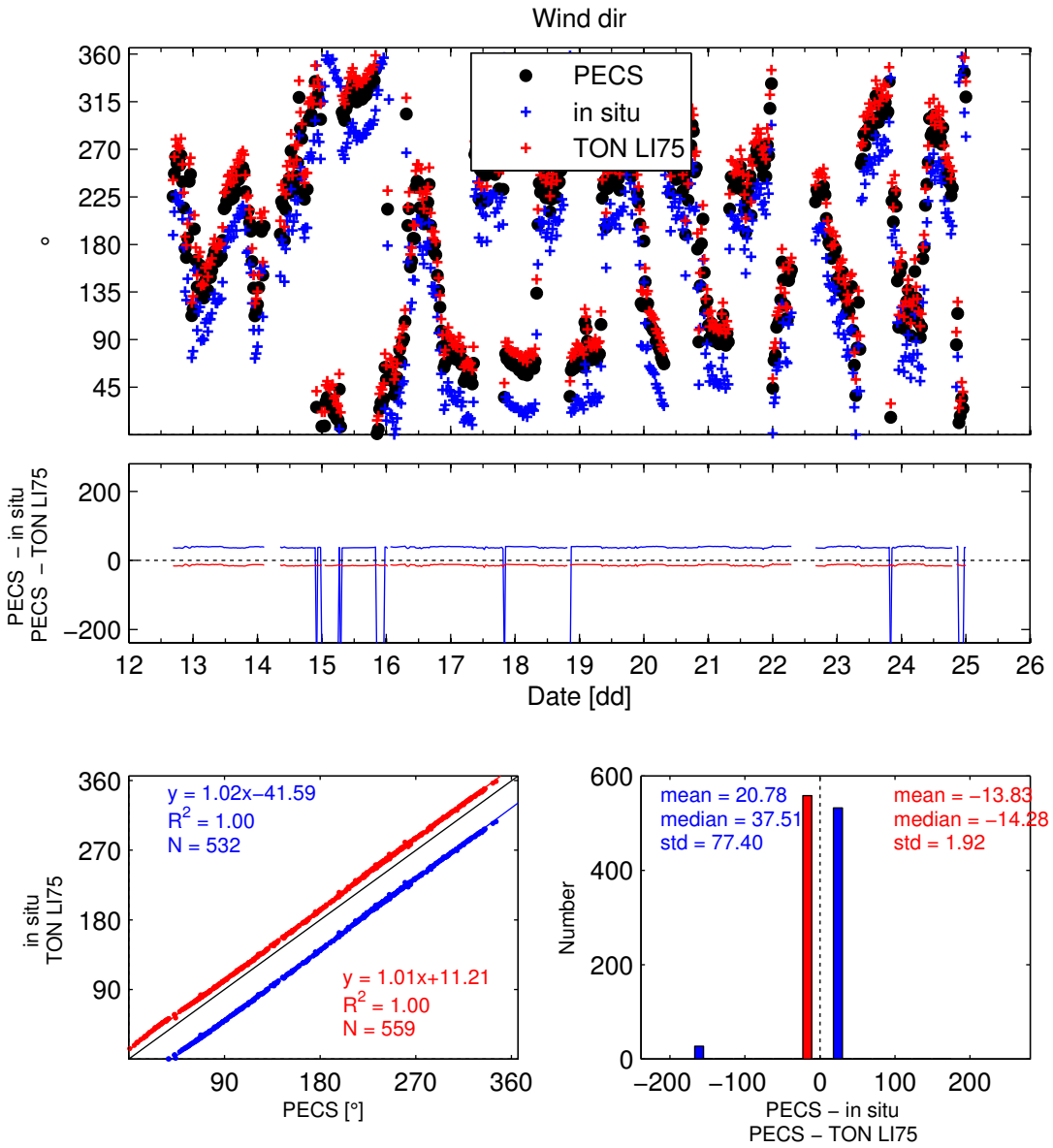

Figure 21 – Wind direction comparison between PECS2, *in situ* data and independently processed raw *in situ* data.

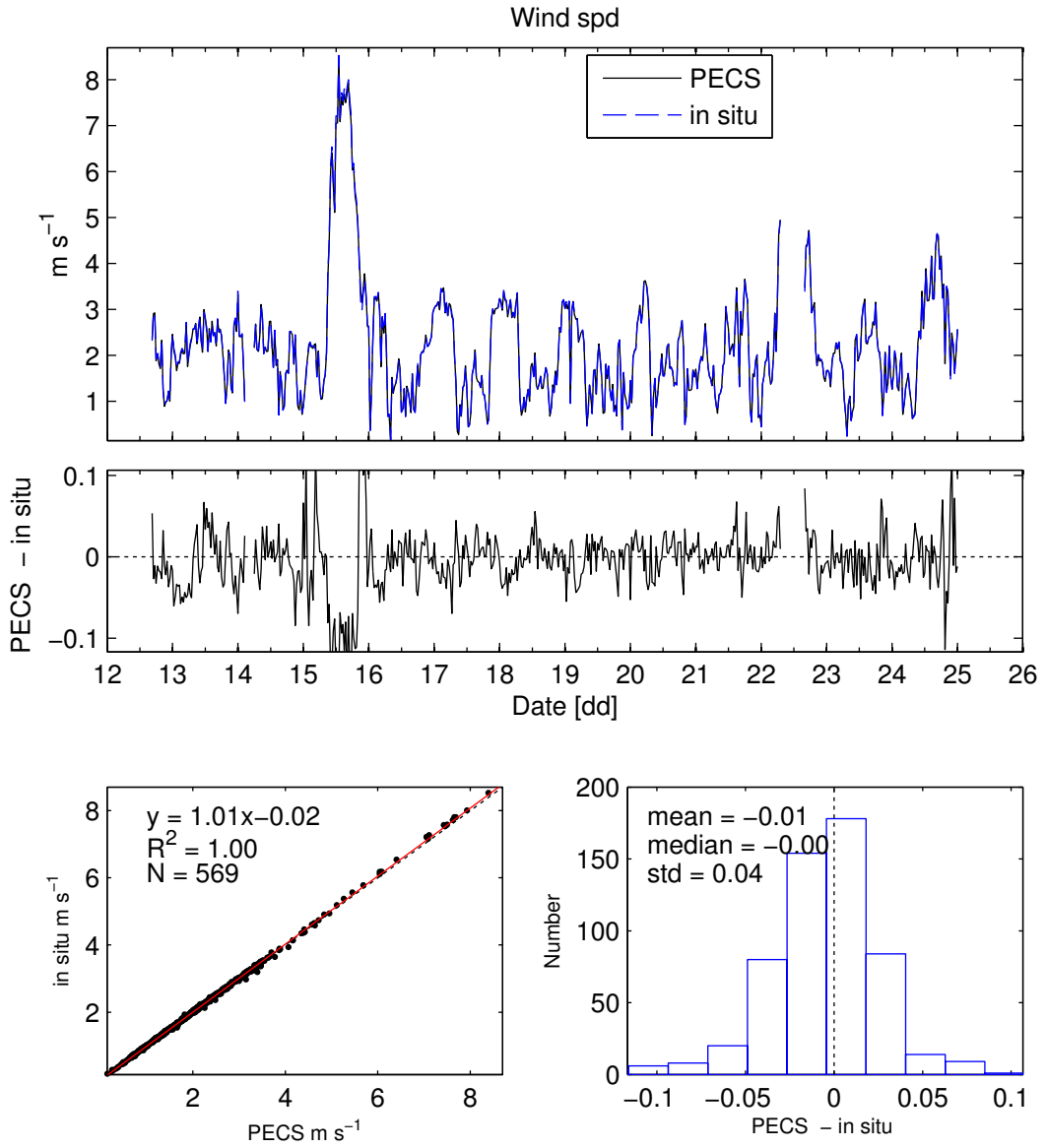

Figure 22 – Wind speed

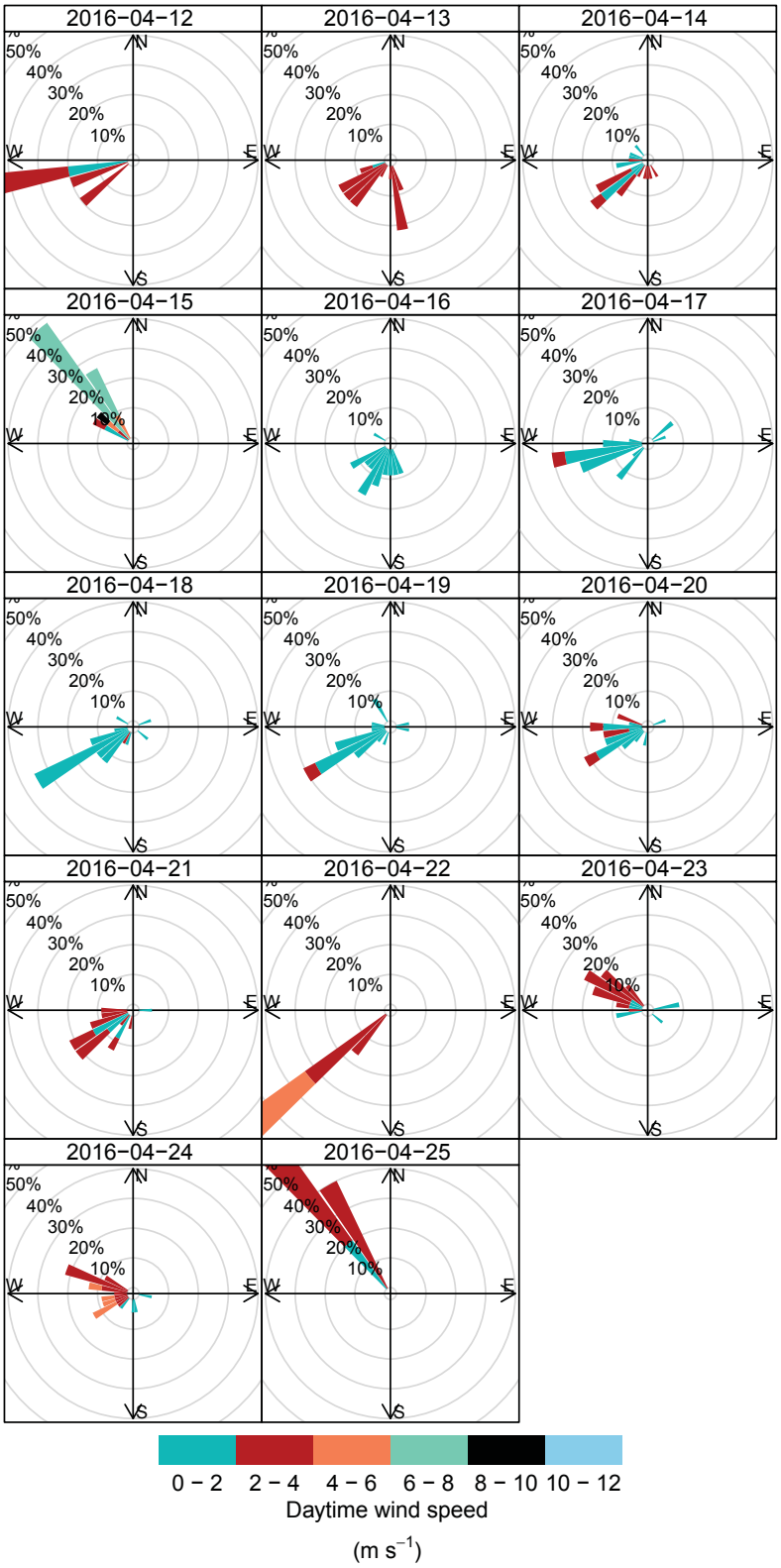

Figure 23 – Wind speed according to wind direction for daytime hours (07:00 -18:30).

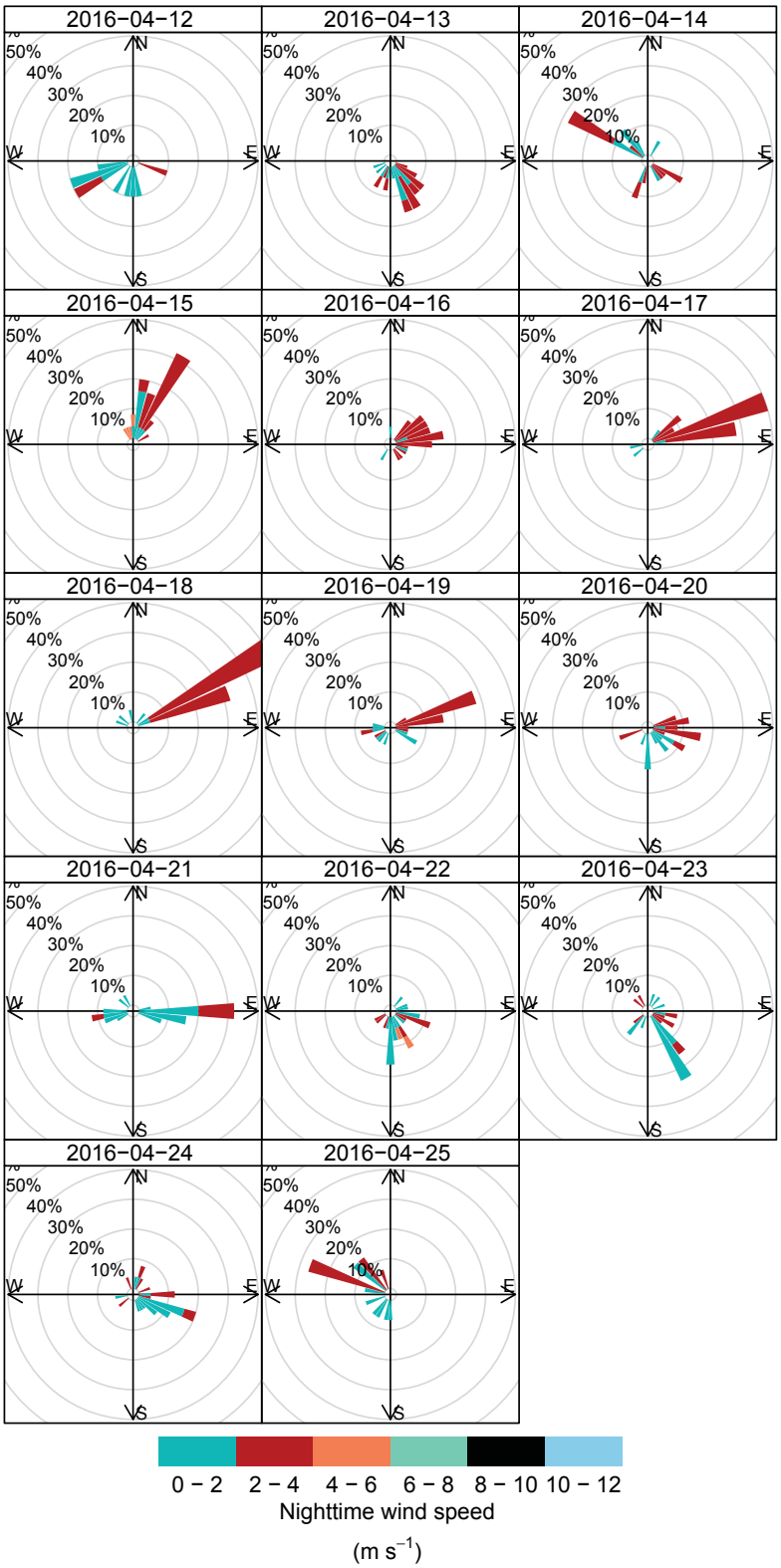

Figure 24 – Wind speed according to wind direction for nighttime hours (19:00 -06:30).

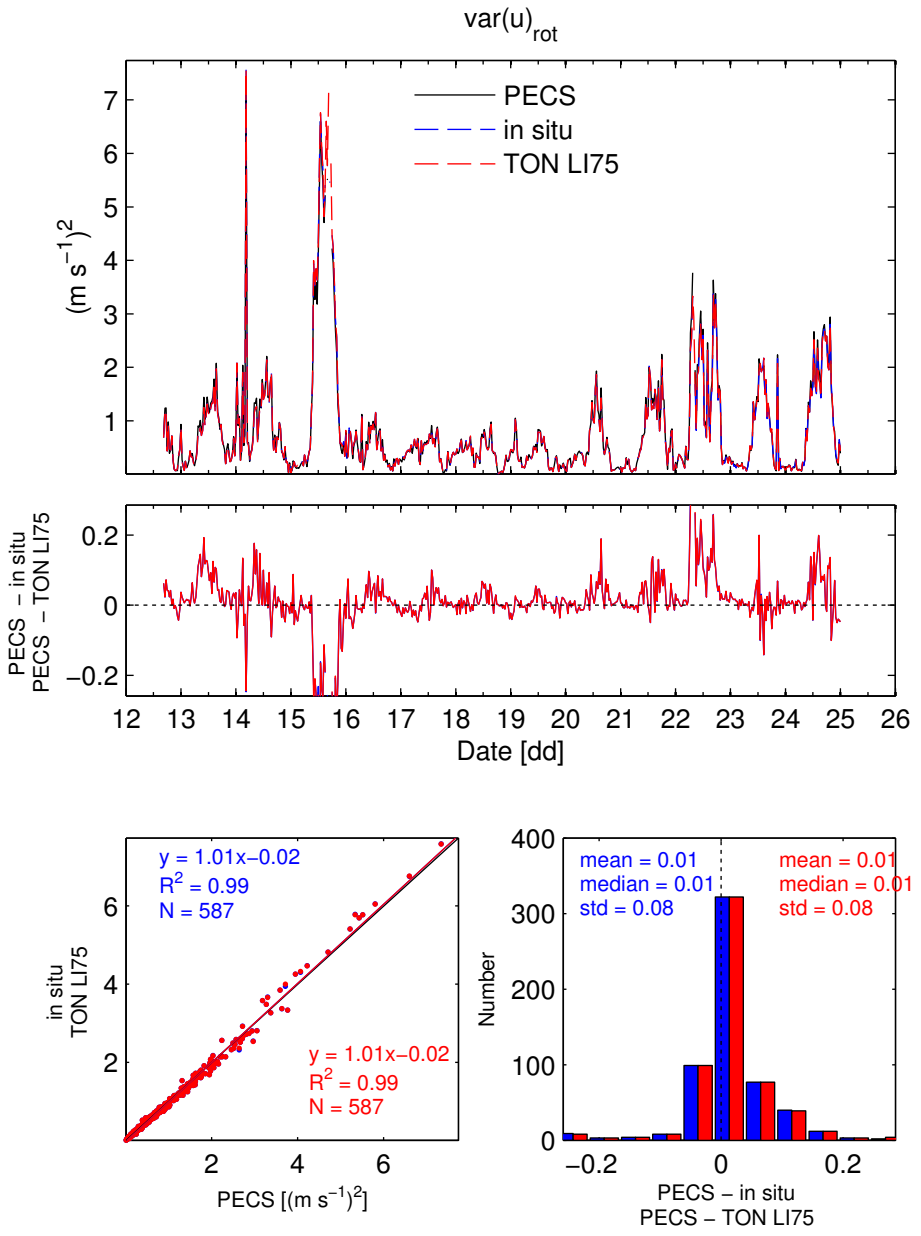

Figure 25 – Rotated u-wind component variance.

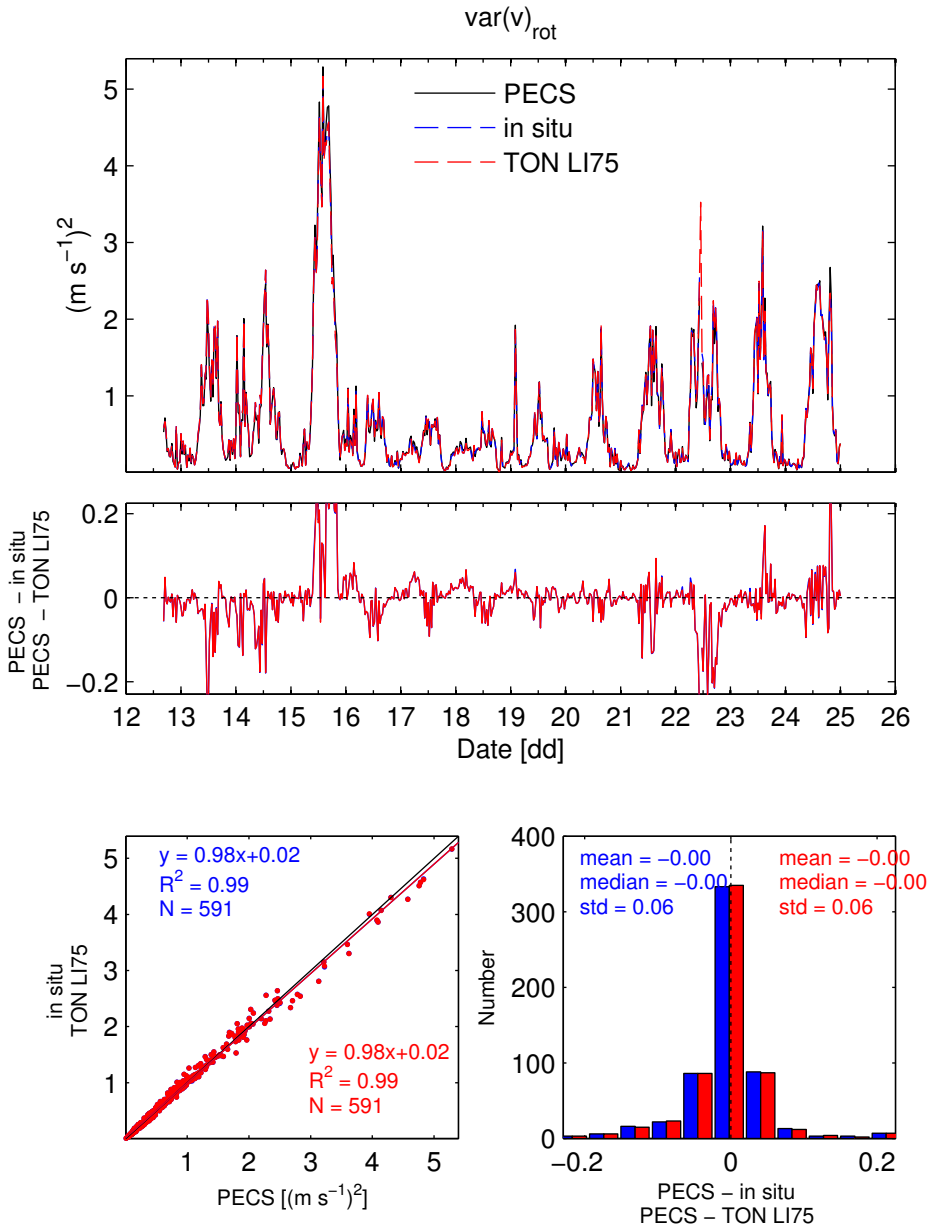

Figure 26 – Rotated v-wind component variance.

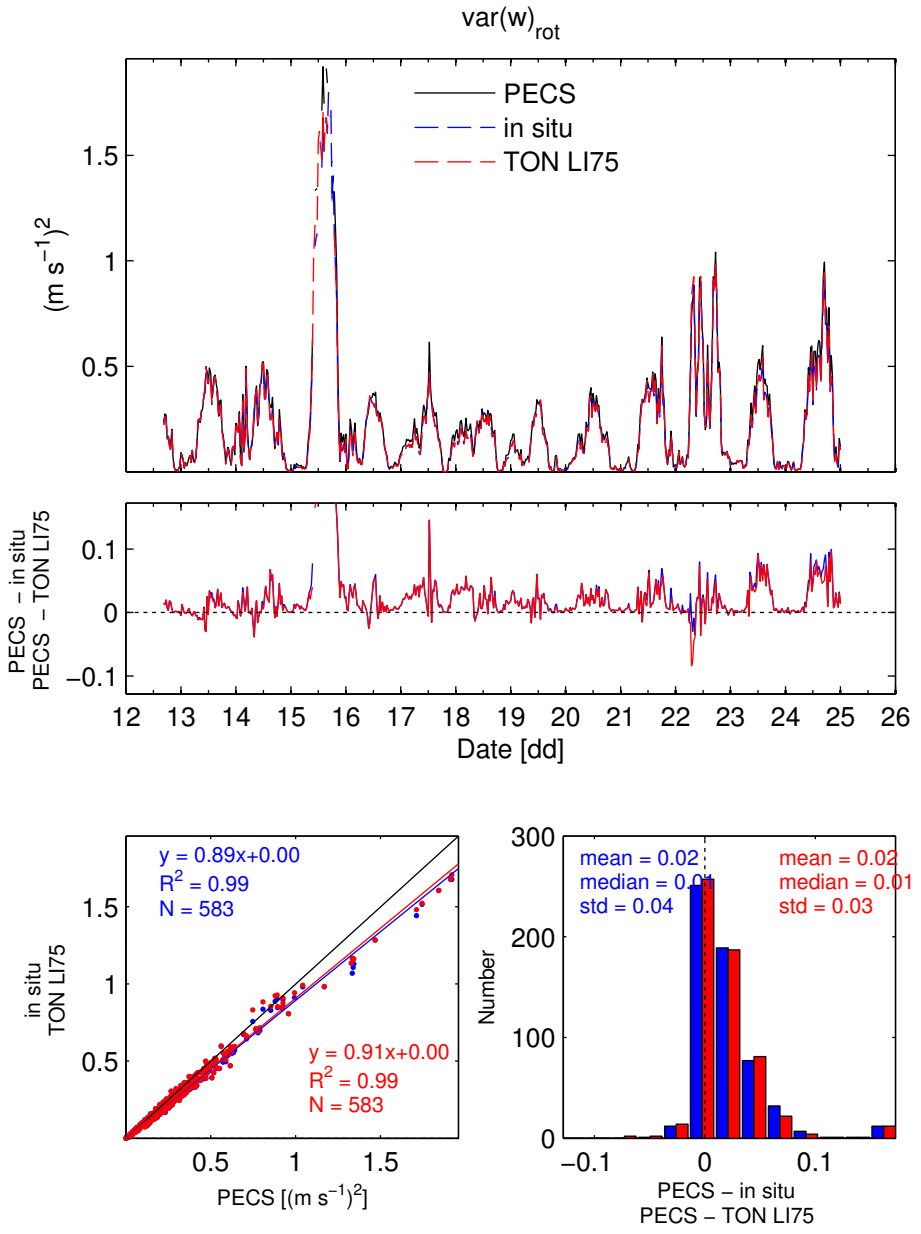

Figure 27 – Rotated w-wind component variance.

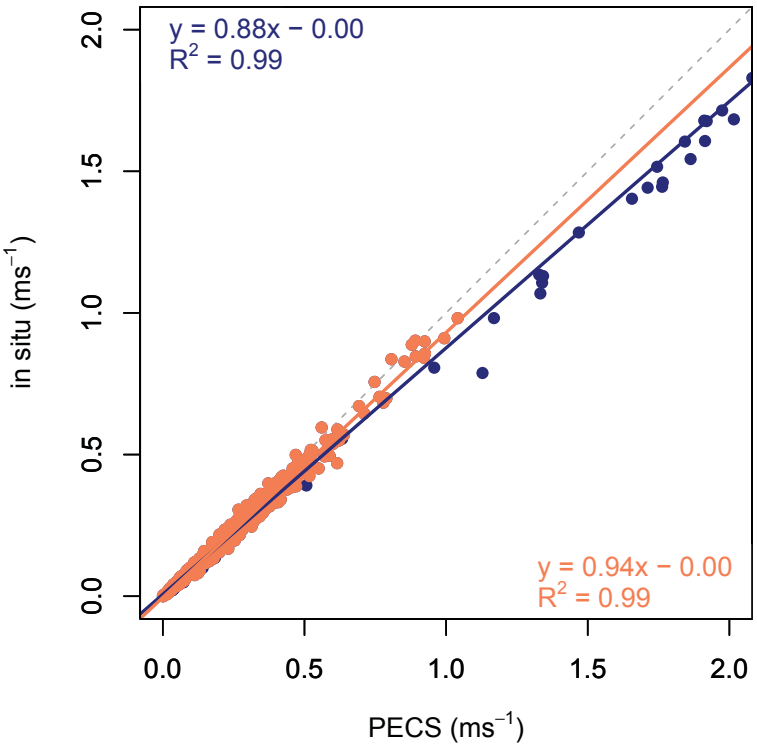

Figure 28 – Rotated w-wind component variance for the entire period and excluding values from 15. April (exceptionally high wind speeds).

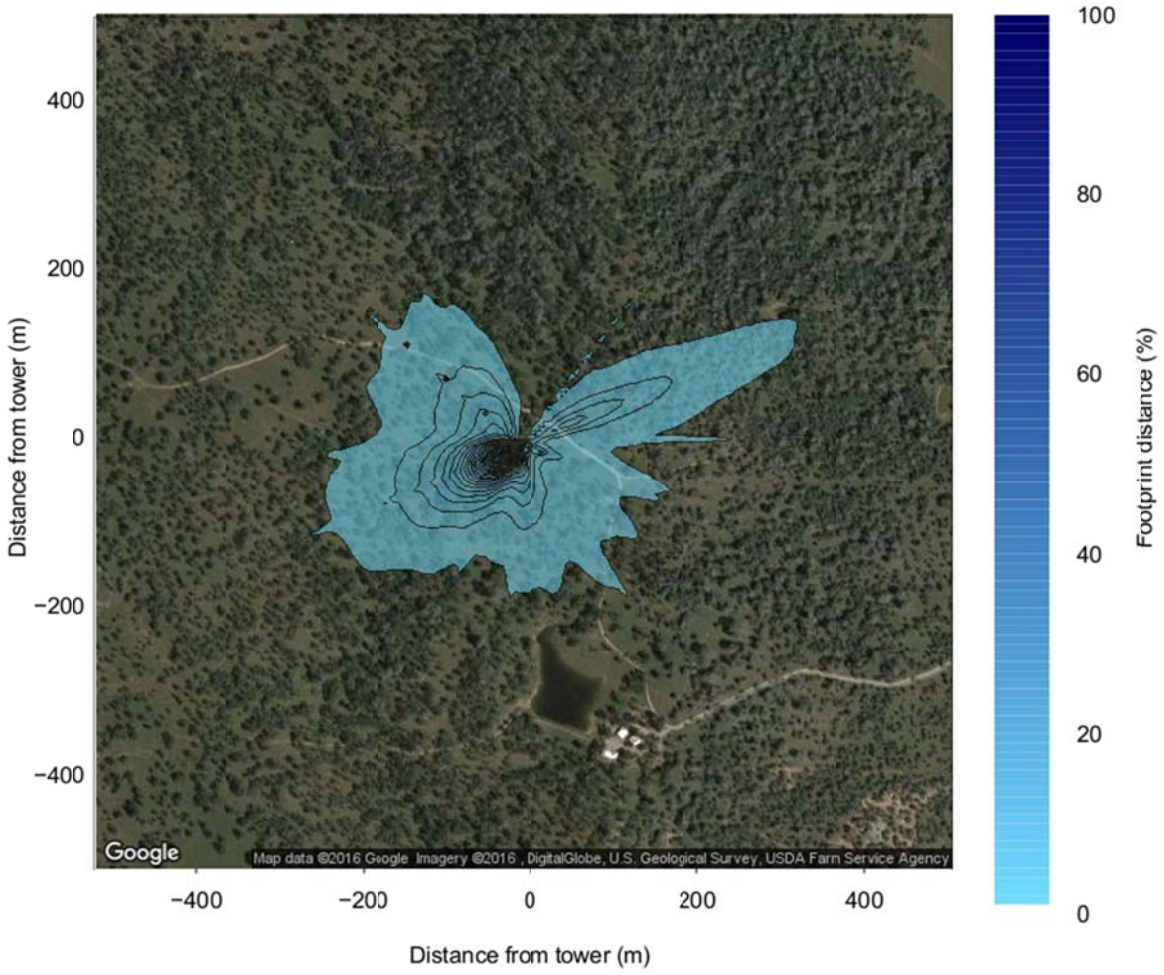

Figure 29 – Averaged footprint distribution (Kormann & Meixner, 2001) for the entire site visit measurement period.

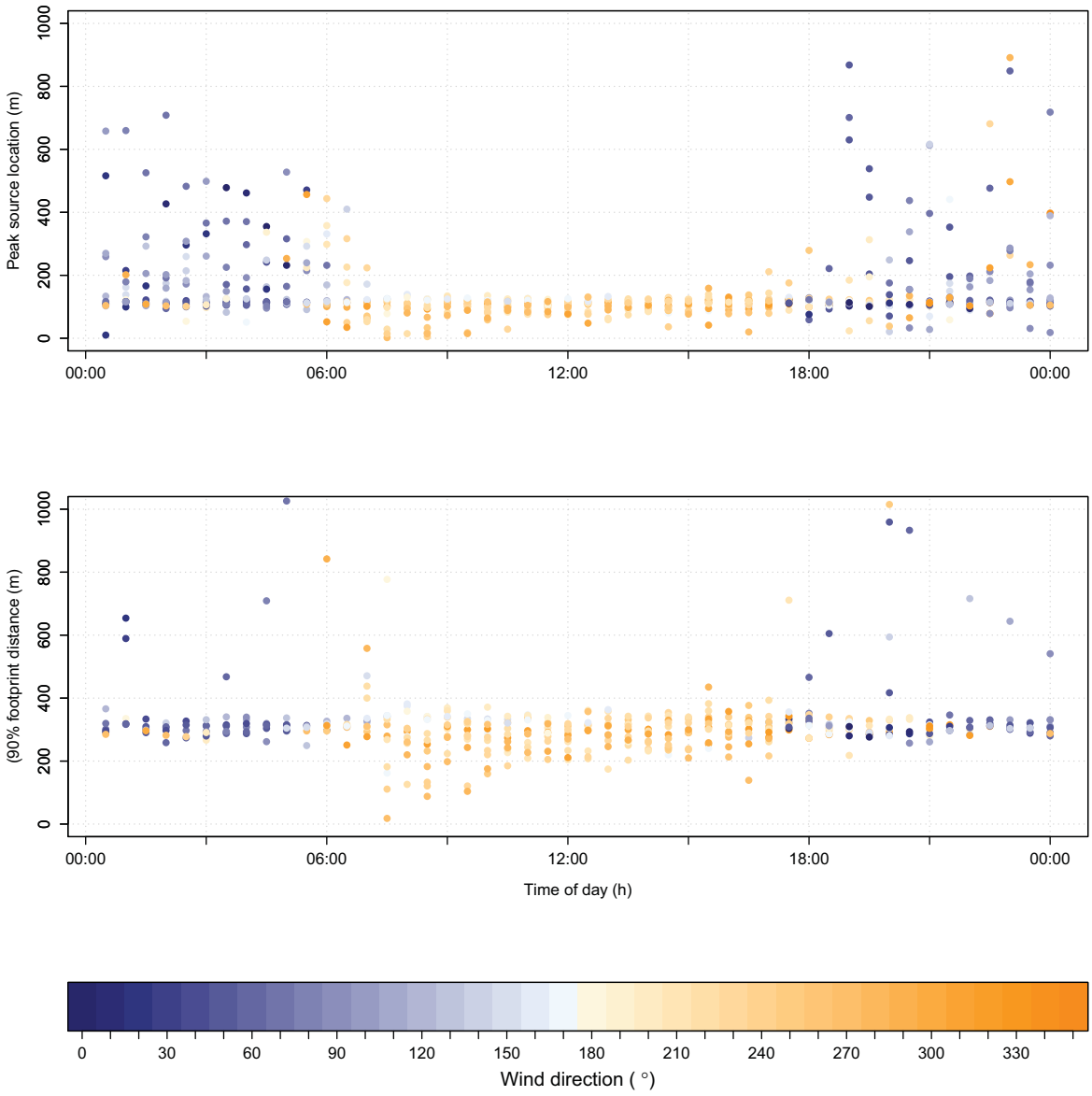

Figure 30 – Diurnal distribution of the maximum footprint source location and 90% footprint contribution distance in upwind direction calculated from PECS2 data.

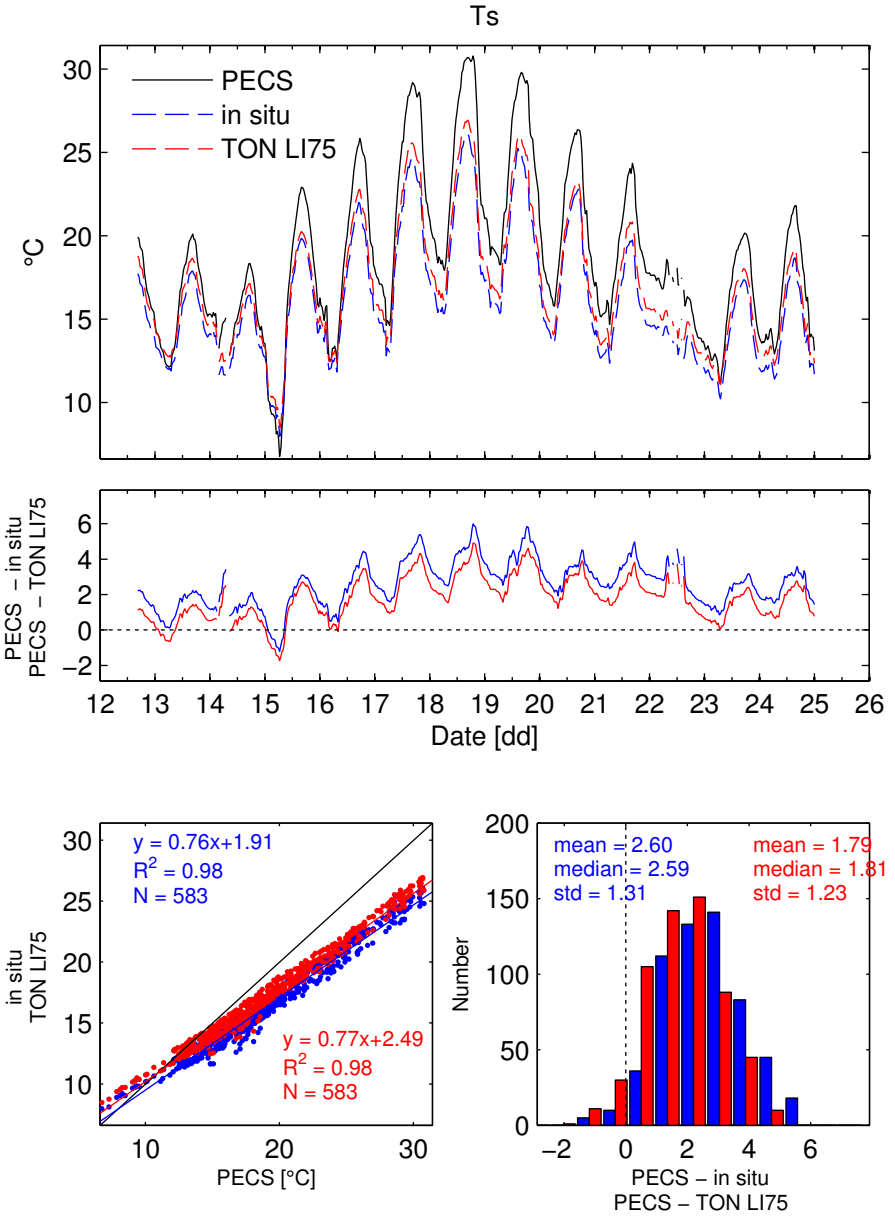

Figure 31 – Mean sonic temperature.

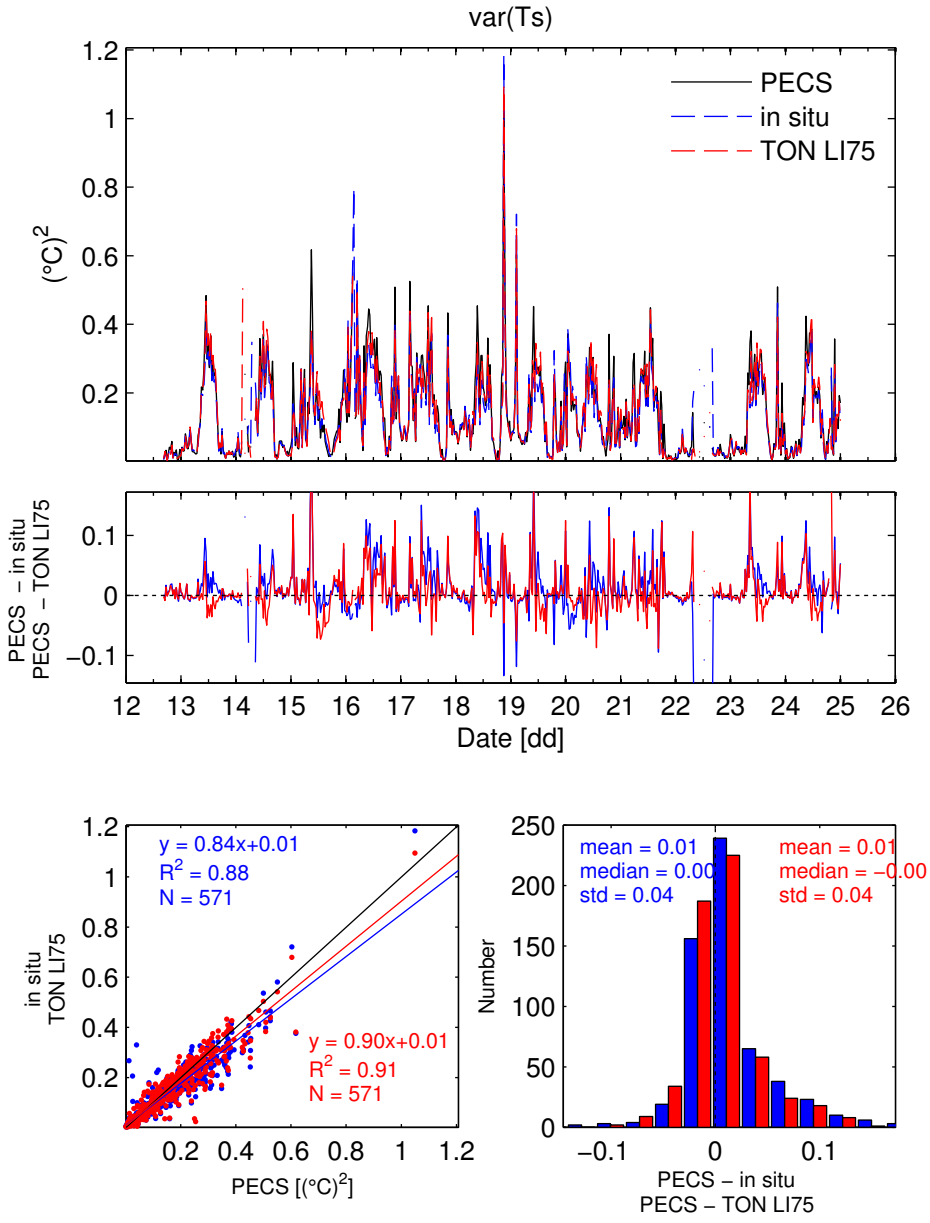

Figure 32 – Sonic temperature variance.

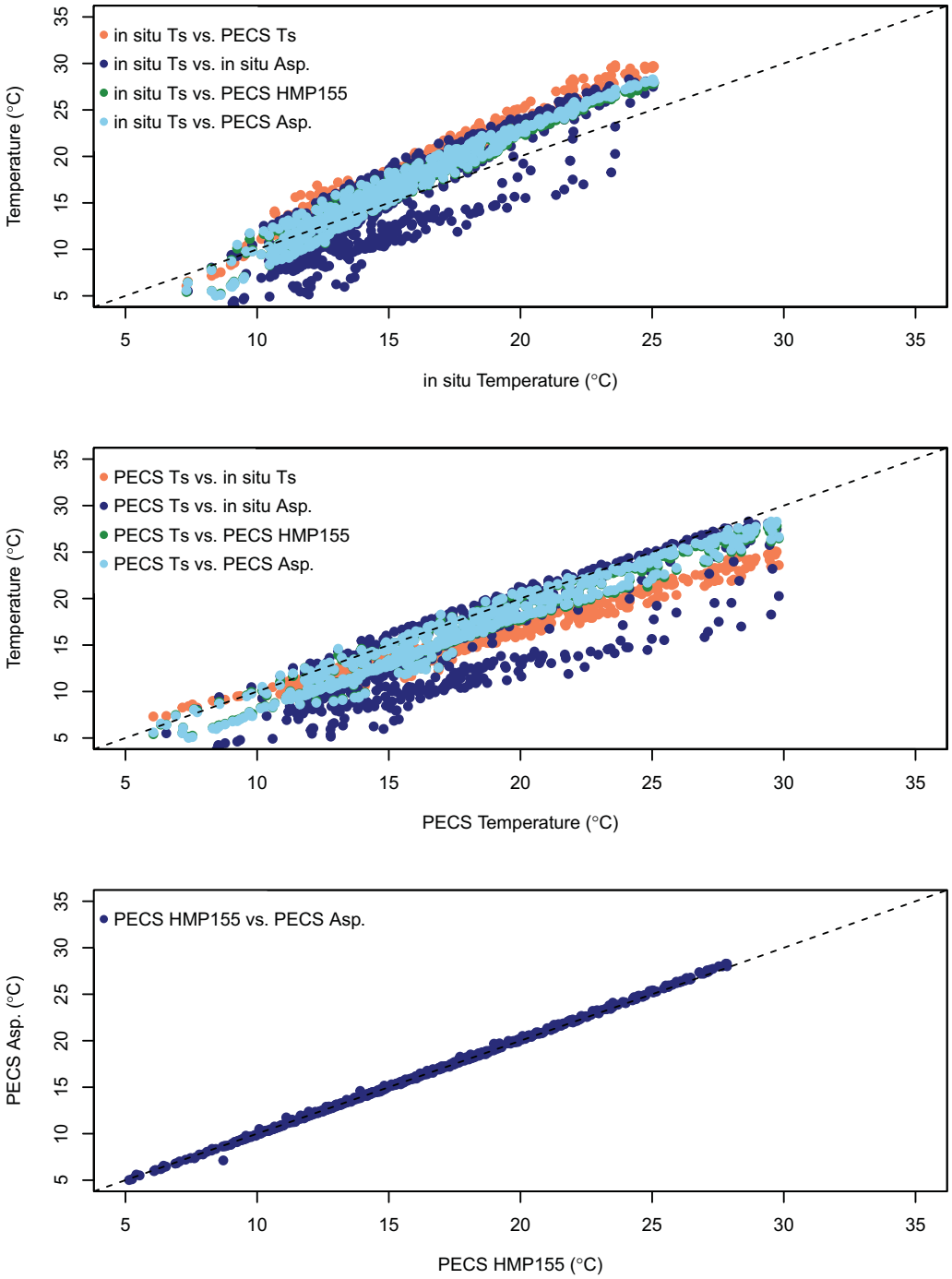

Figure 33 – Comparison between the mean converted (to true temperature) sonic temperature and a variety of ambient air temperature measurements. “Asp.” stands for aspirated temperature sensor, which in case of PECS2 is a R.M. Young probe. Included is also the comparison between both PECS2 ambient air temperature measurements: HMP155 and the aspirated RM Young probe.

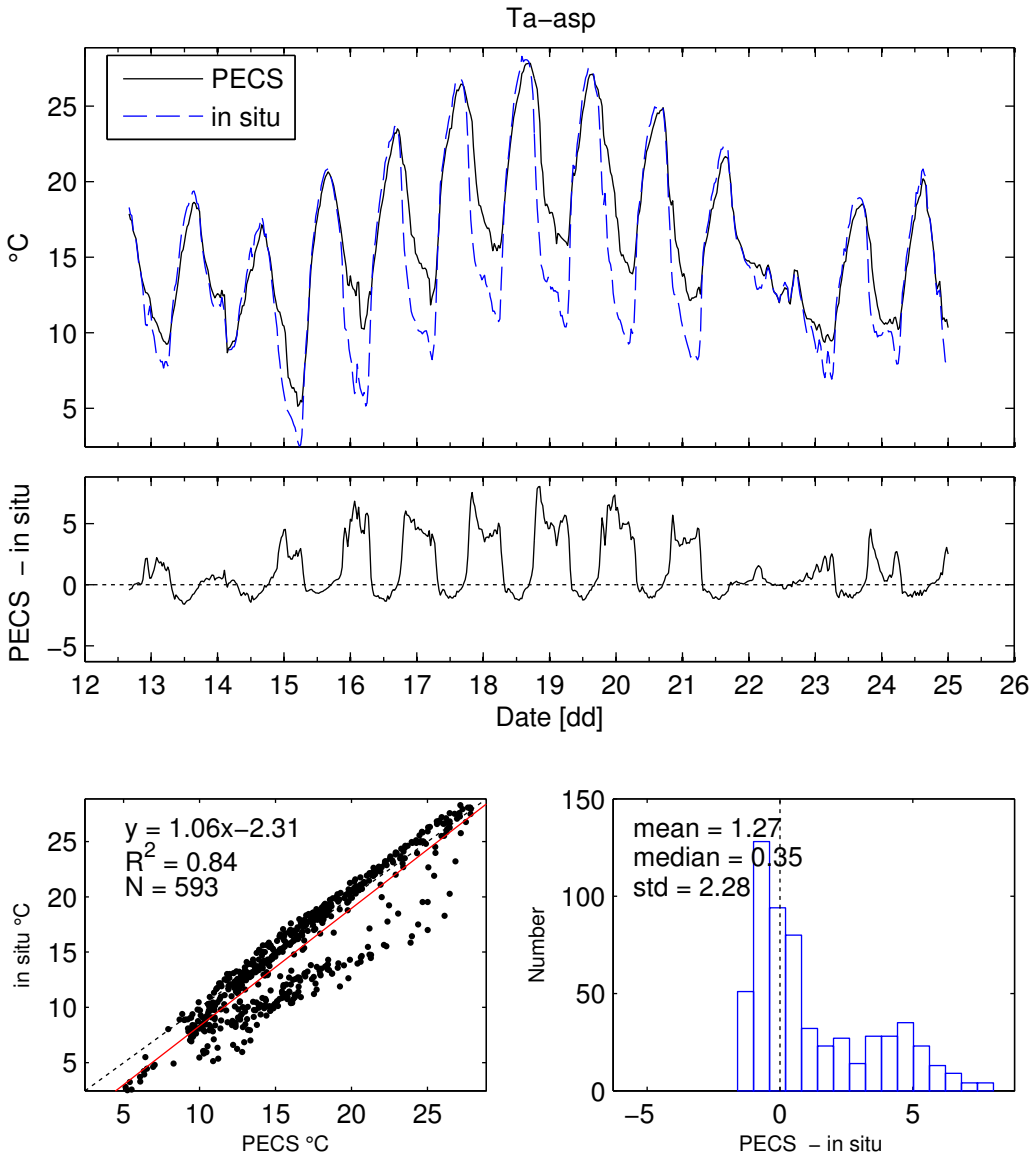

Figure 34 – Ambient air temperature.

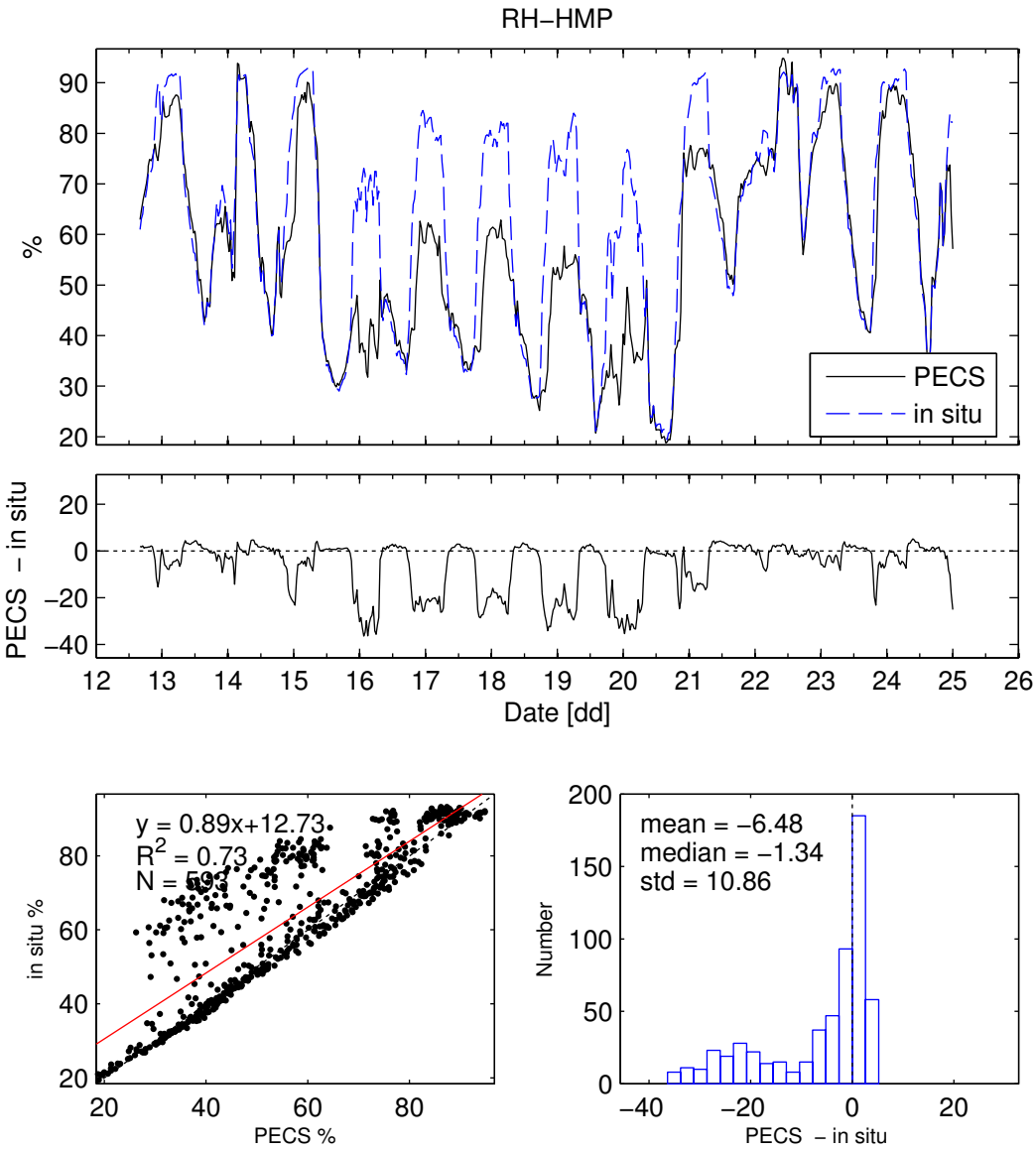

Figure 35 – Relative humidity.

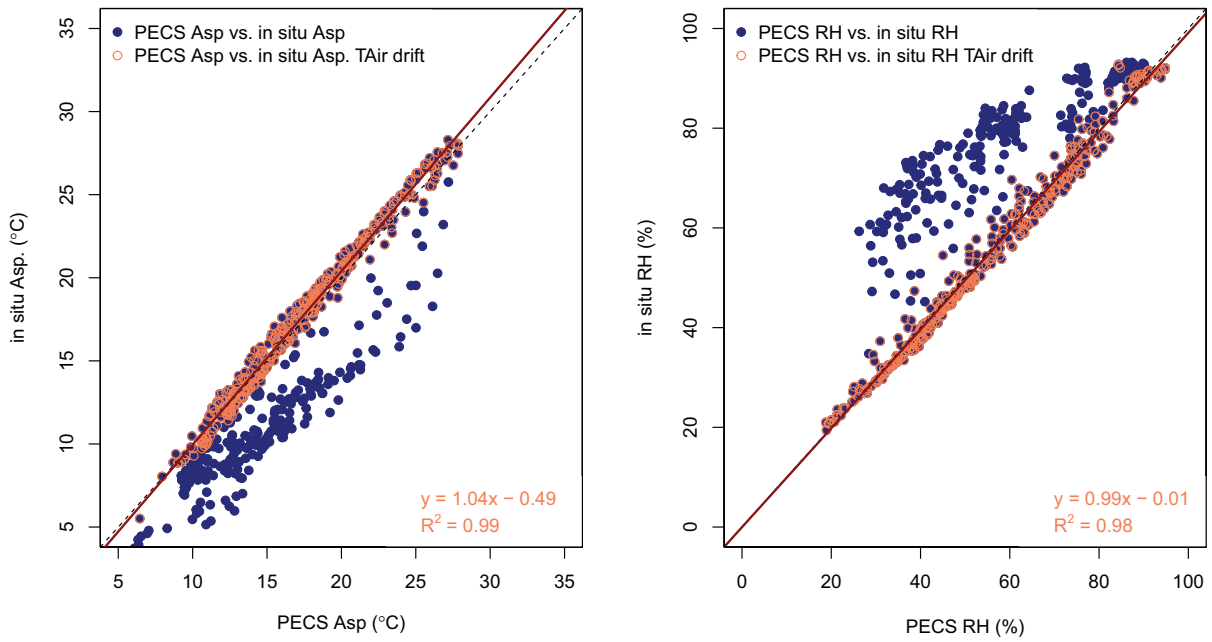

Figure 36 – Comparison between the PECS2 HMP155 and the *in situ* HMP45. Blue values represent all data from the respective probe, while orange marked values highlight those values with a discrepancy of less than 2°C.

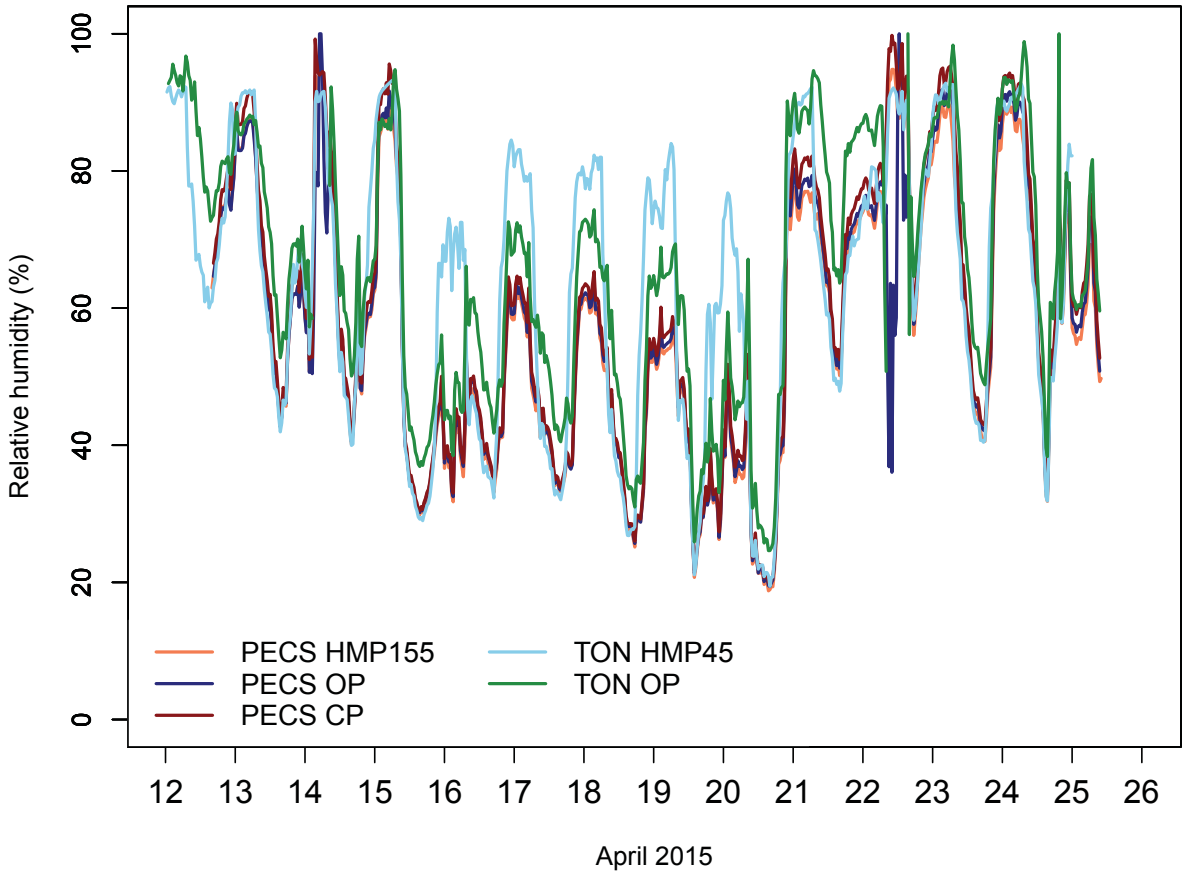

Figure 37 – Relative humidity estimated from both HMP probes as well as all three gas analyzers.

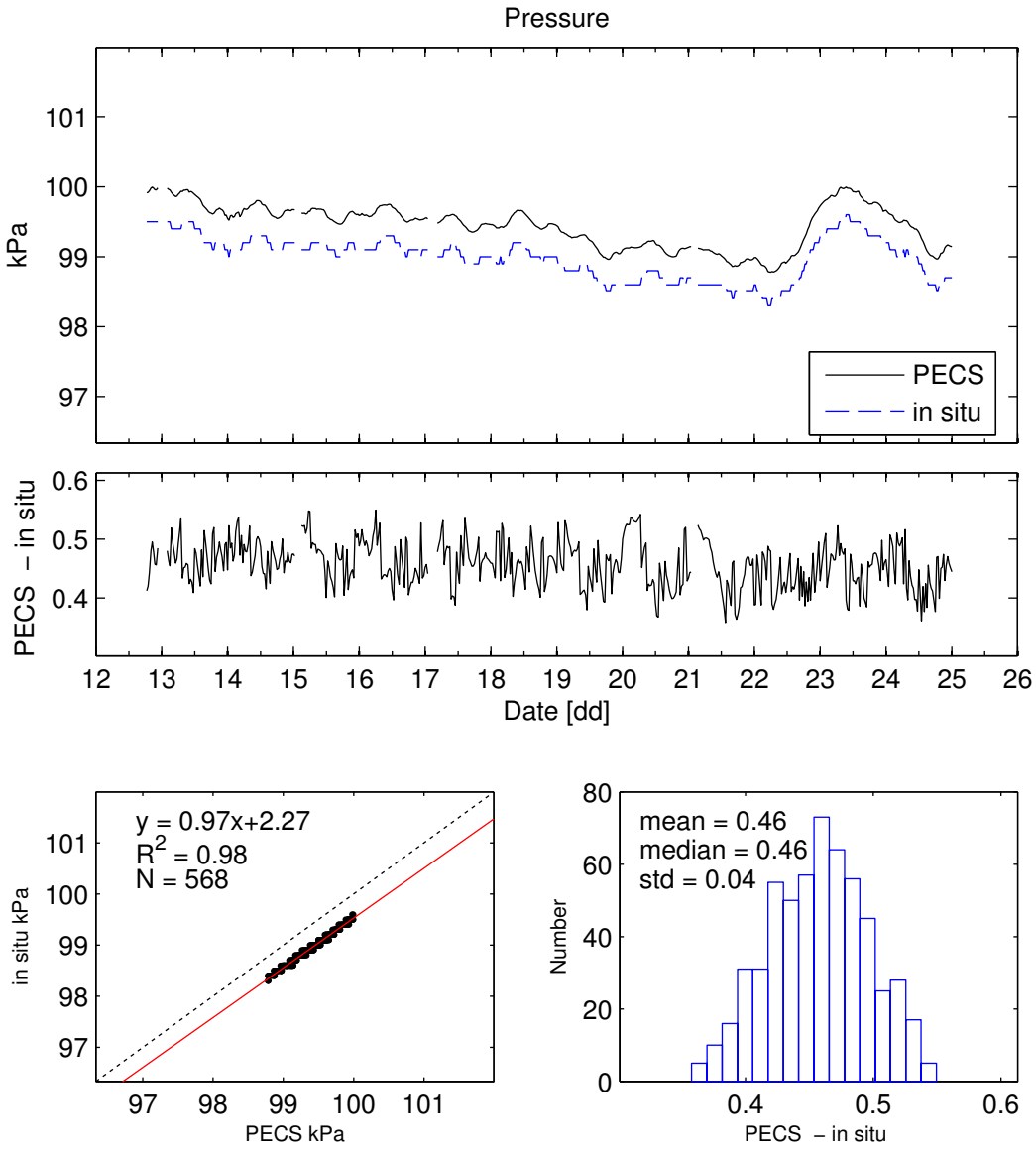

Figure 38 – Atmospheric pressure.

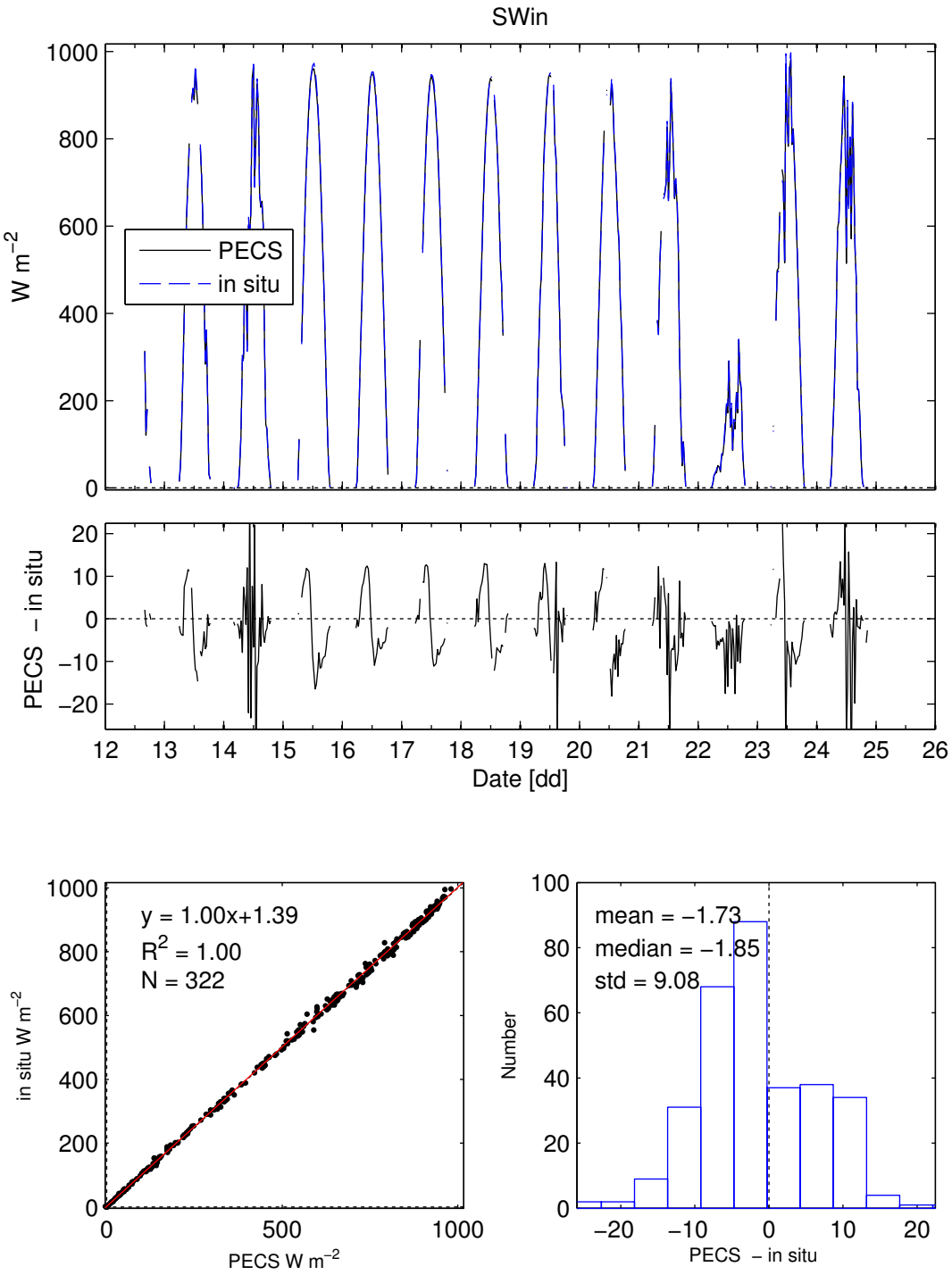

Figure 39 – Incoming shortwave radiation.

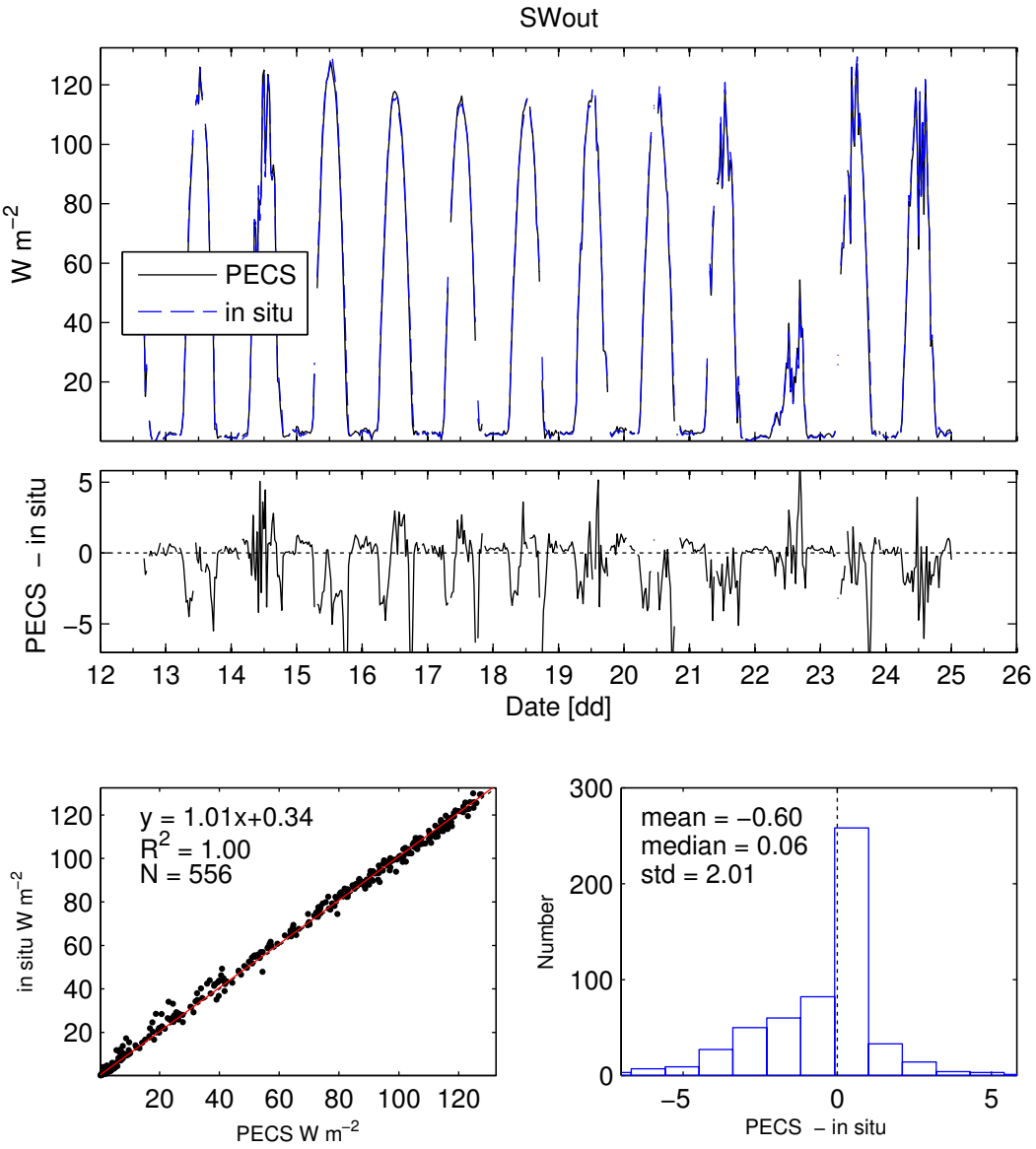

Figure 40 – Outgoing shortwave radiation.

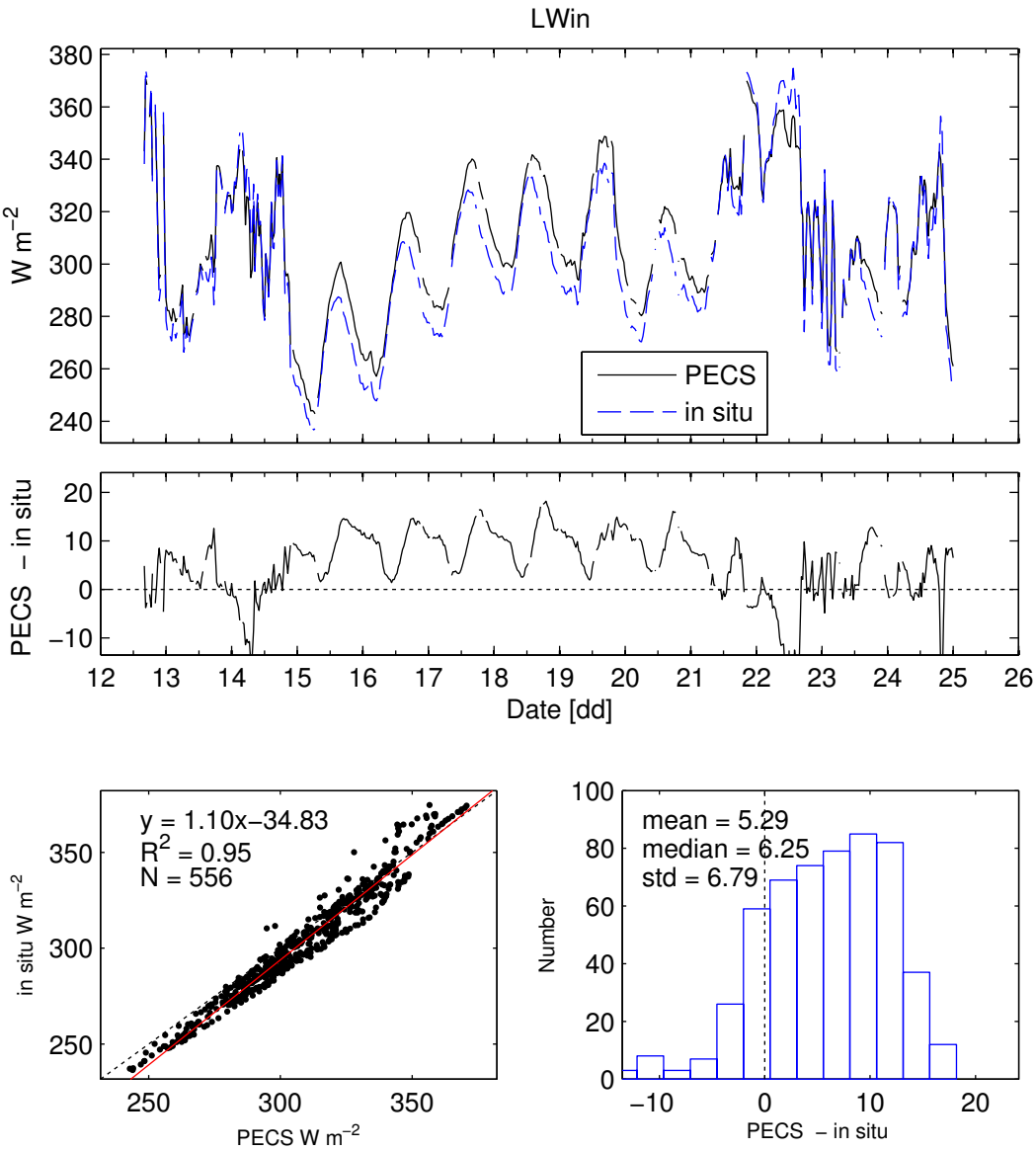

Figure 41 – Incoming longwave radiation.

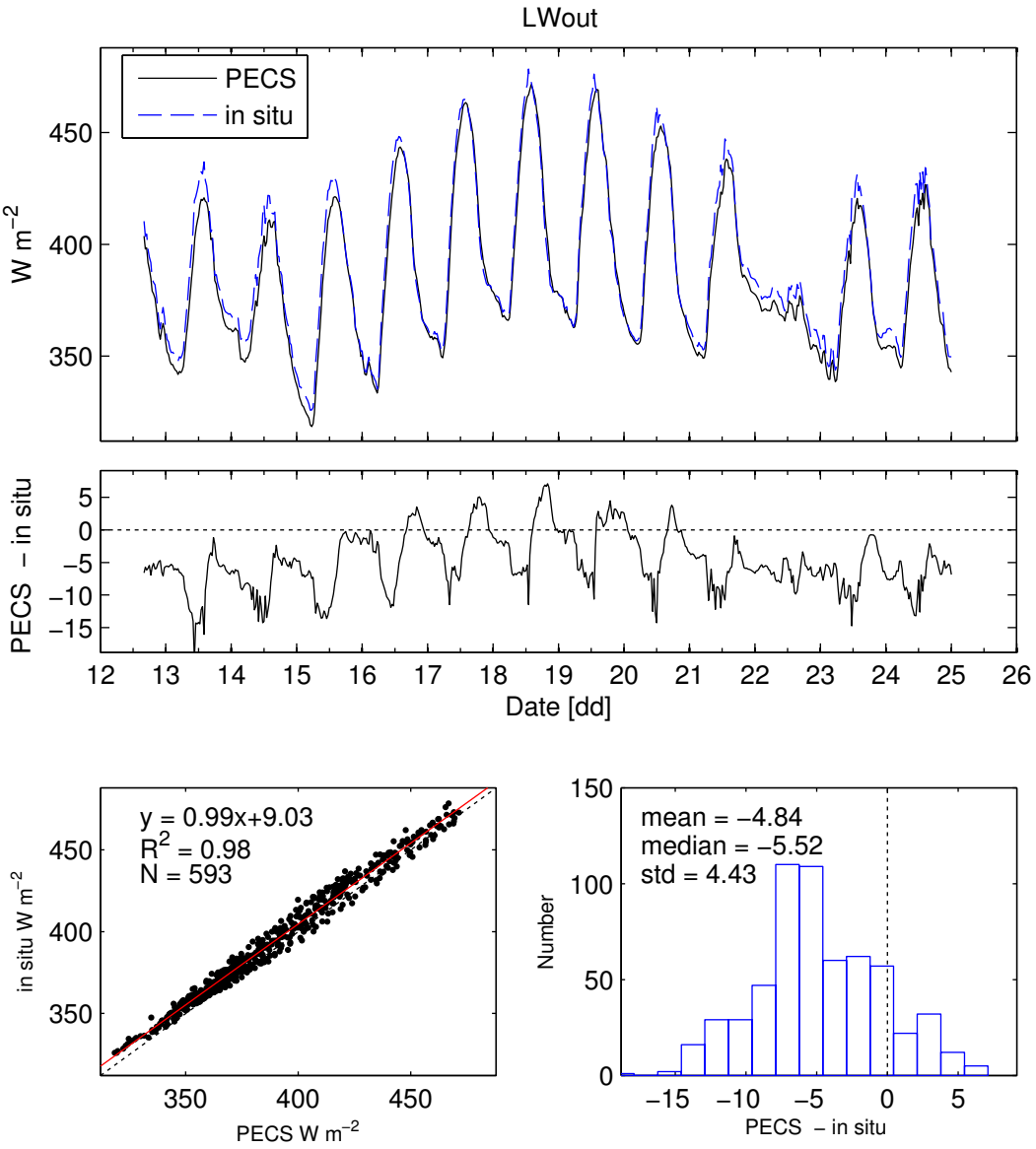

Figure 42 – Outgoing longwave radiation.

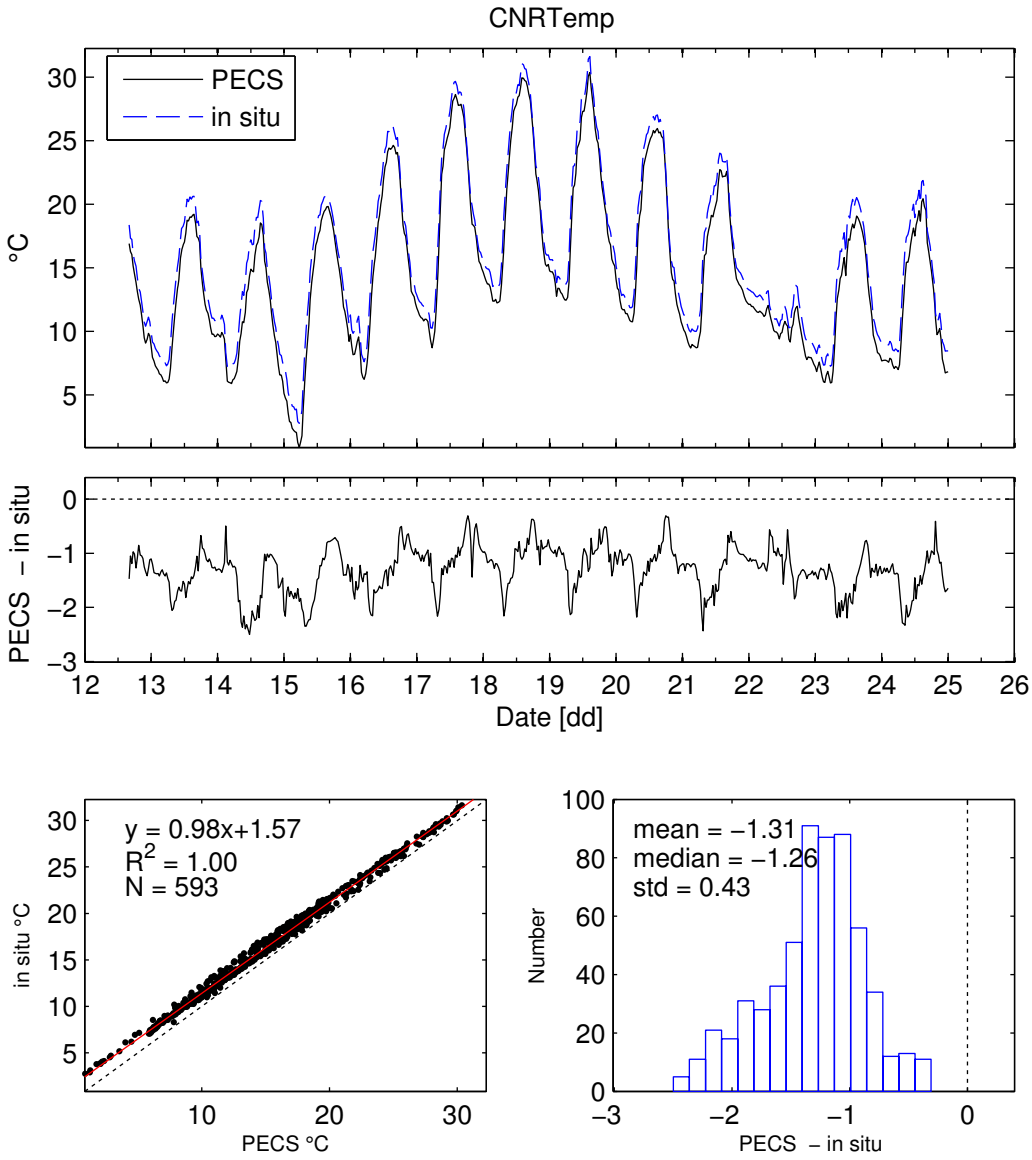

Figure 43 – Instrument body temperatures of the CNR4 (PECS2) and the *in situ* CNR1.

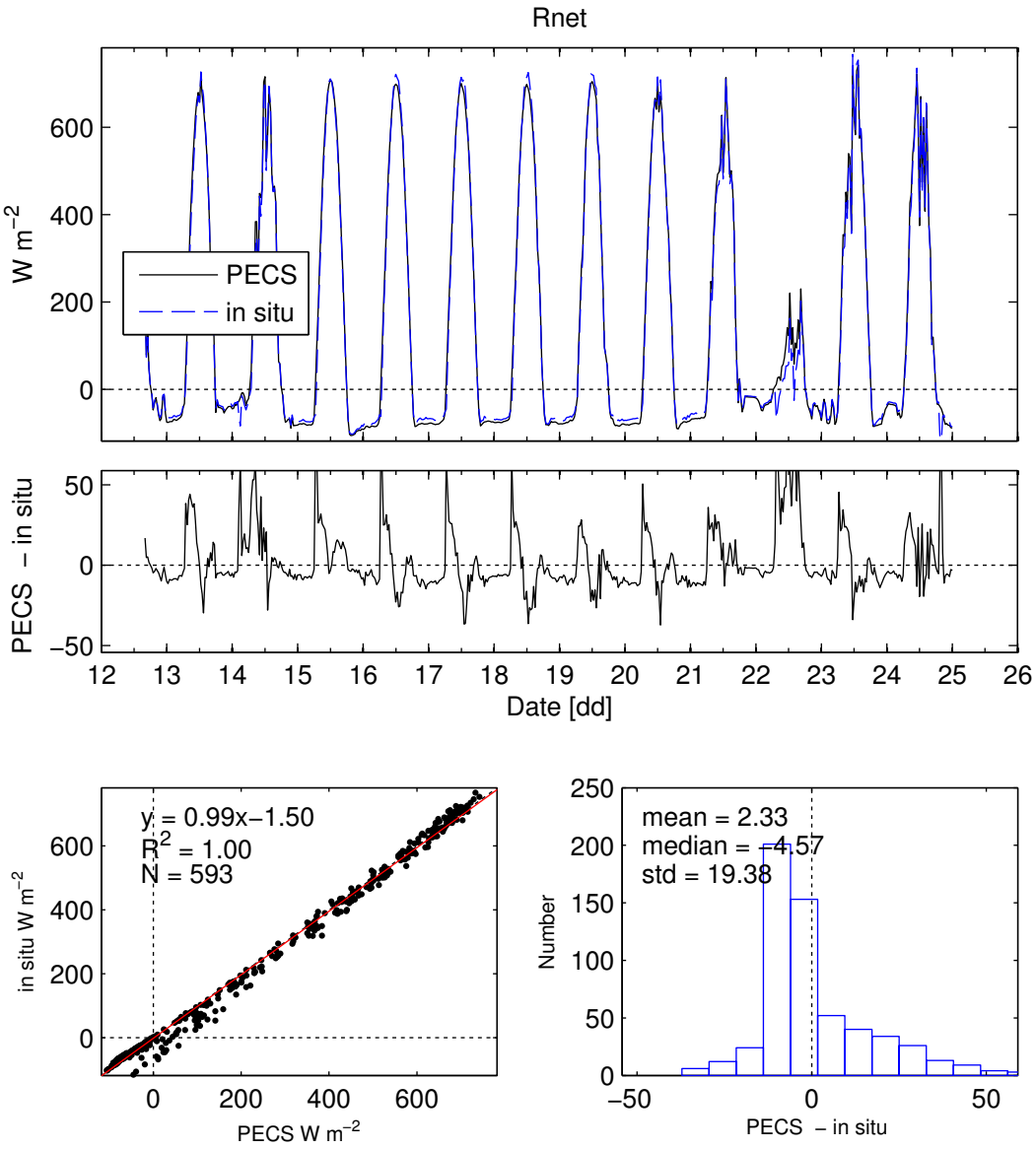

Figure 44 – Net radiation.

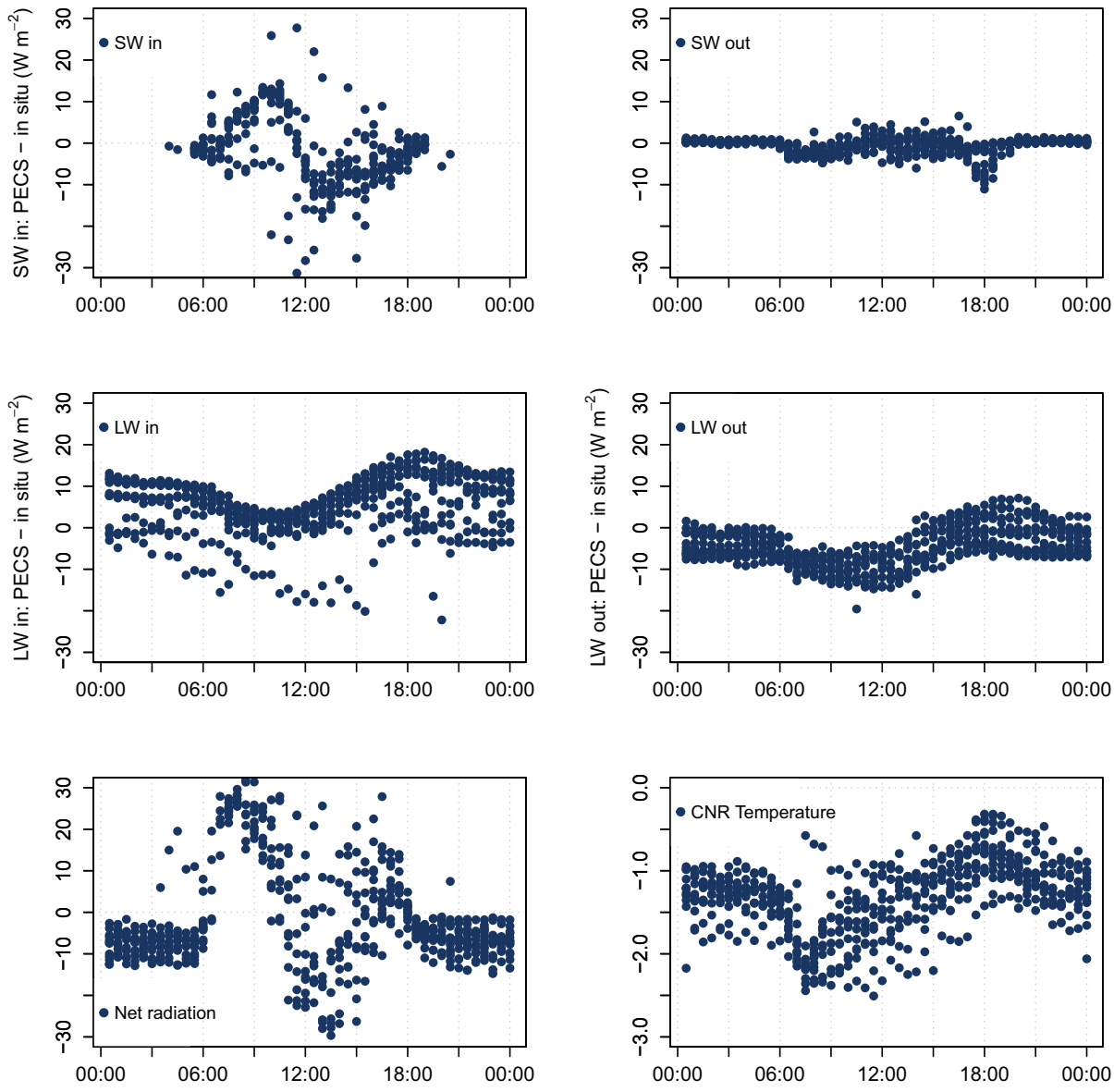

Figure 45 –Discrepancies in individual CNR4/CNR1 radiation components by time of day.

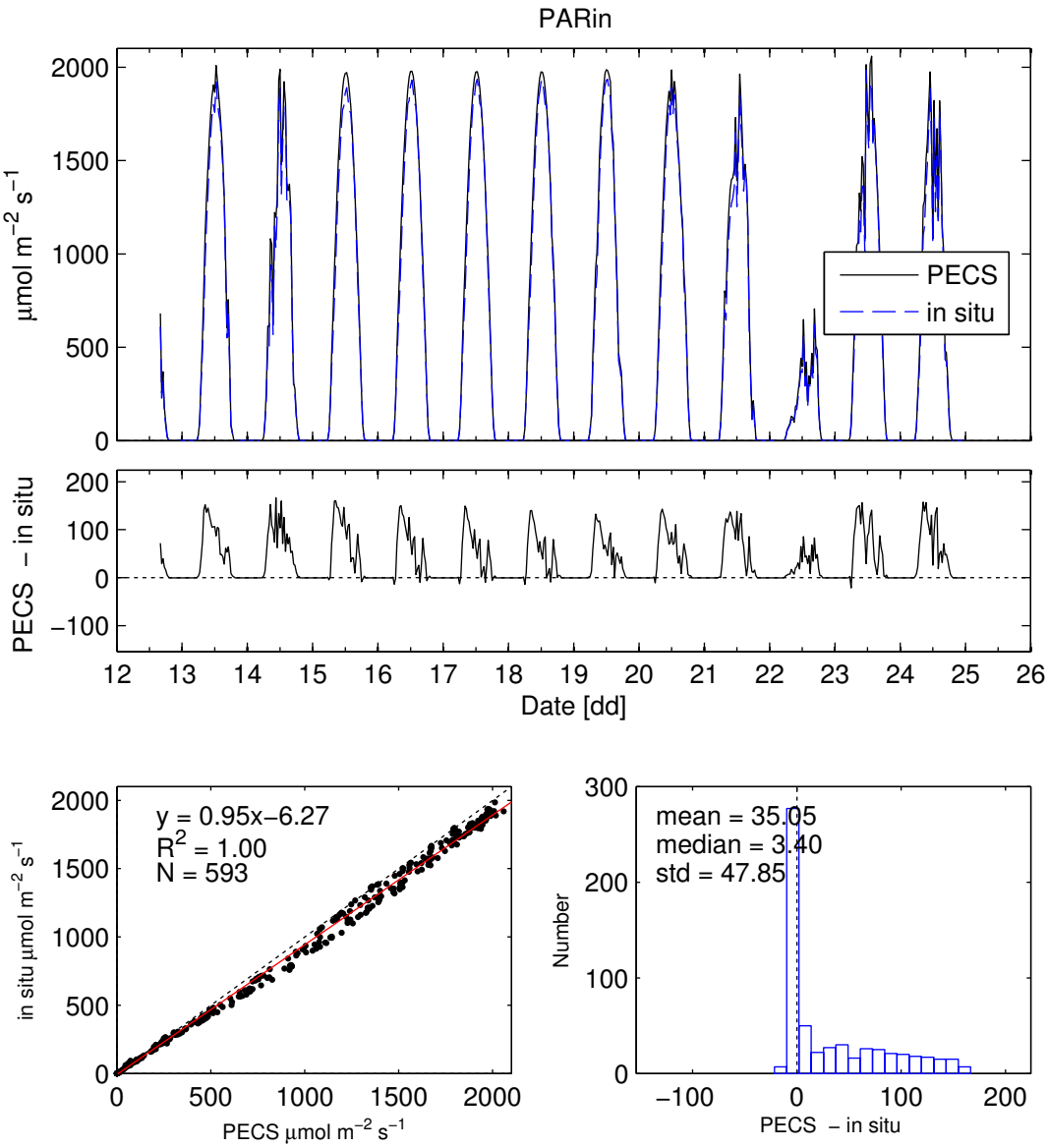

Figure 46 – Incoming photosynthetically active radiation (PAR).

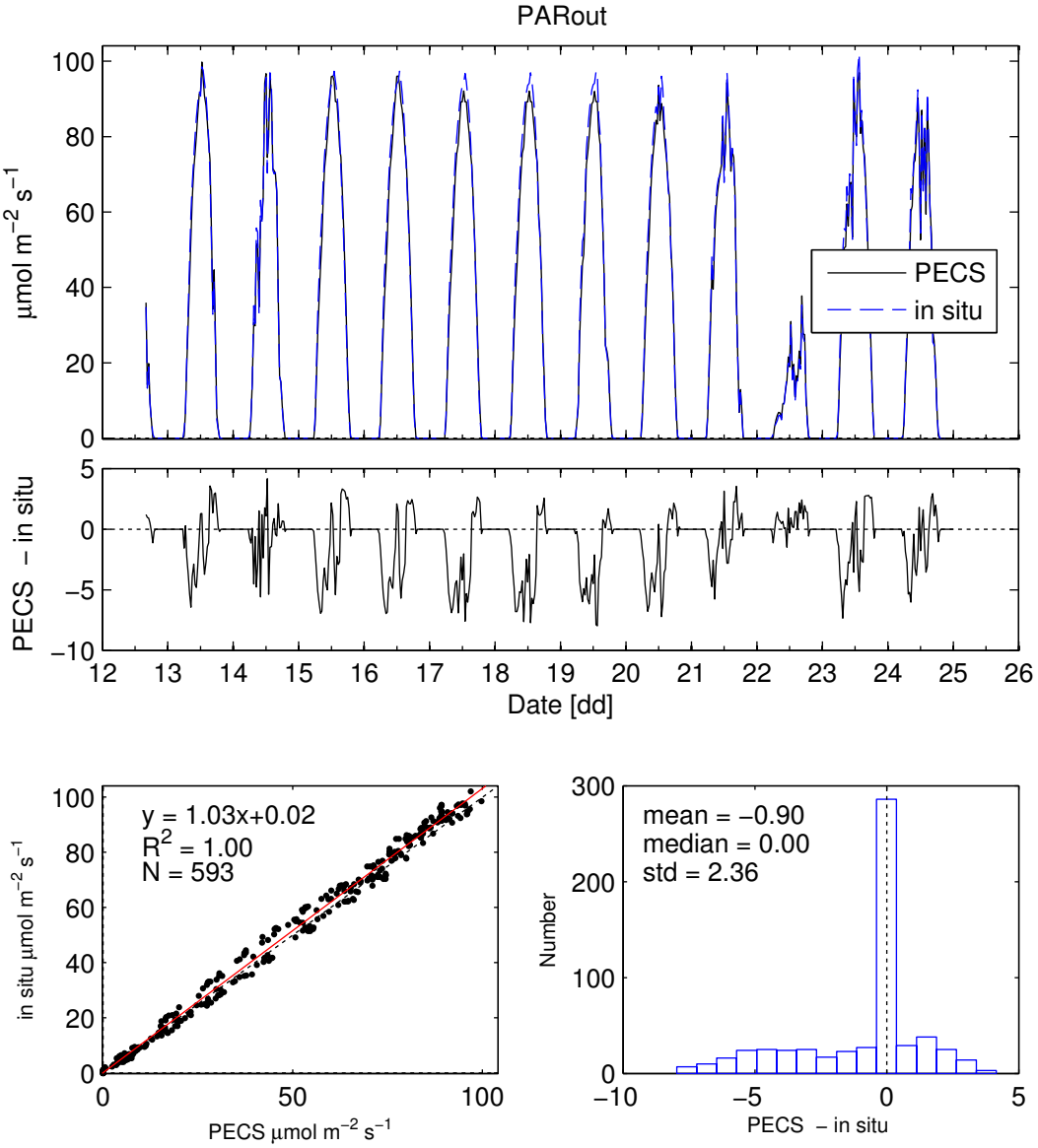

Figure 47 – Outgoing photosynthetically active radiation (PAR).

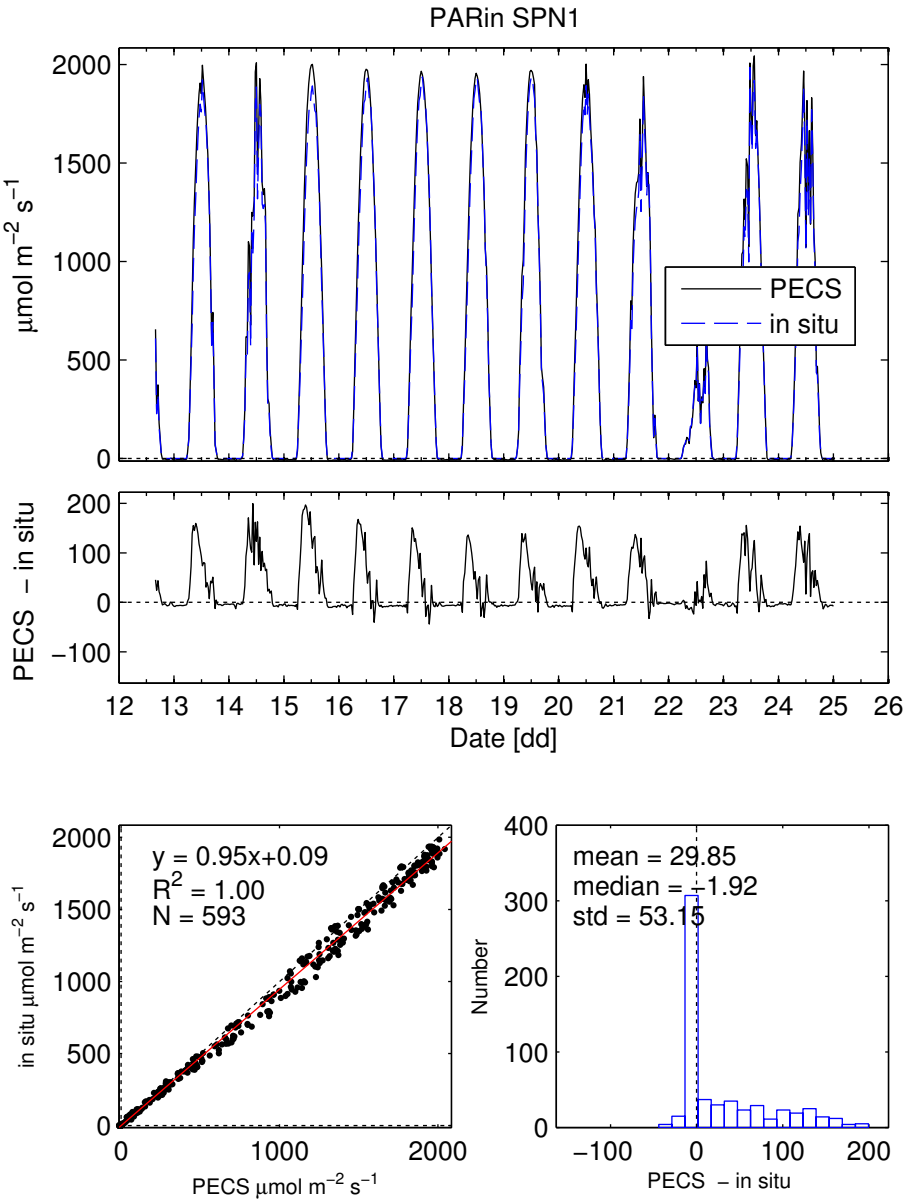

Figure 48 –Global photosynthetic active radiation measured with the in situ Delta-T BF5 and approximated values from the Delta-T SPN1 pyranometer.

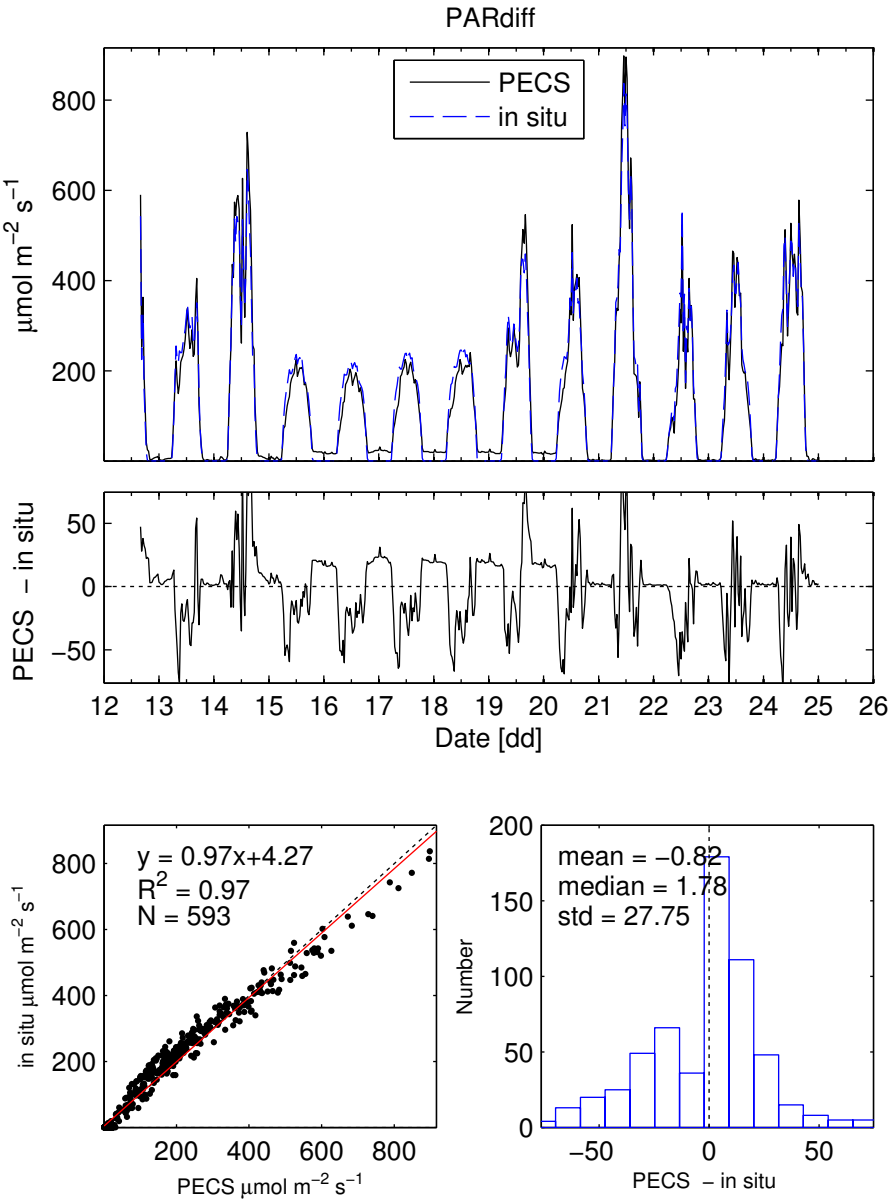

Figure 49 – Diffuse photosynthetic active radiation measured with the in situ Delta-T BF5 and approximated values from the Delta-T SPN1 pyranometer.

Site Name: Tonzi Ranch (US-Ton)
Visit Dates: 12 – 25 April 2016

Table 1 – Summary of basic statistics from linear regression and for each system of compared variables.

	slope	intercept	R2	N	mean1	std1	max1	min1	mean2	std2	max2	min2
CO2 flux	0.812	-0.24	0.964	488	-2.098	8.247	15.385	-31.982	-1.941	6.817	12.822	-25.147
Latent heat	0.969	-0.41	0.986	483	79.877	109.539	425.039	-41.686	76.883	106.838	454.754	-43.000
S. heat	0.933	-0.10	0.983	488	33.074	84.555	299.543	-111.908	30.790	79.595	276.814	-107.794
u star	0.971	-0.009	0.971	569	0.322	0.213	1.150	0.009	0.304	0.210	1.175	0.015
u_{rot}	1.011	-0.020	0.999	592	2.233	1.269	8.395	0.149	2.238	1.284	8.528	0.167
v_{rot}	0.001	0.000	0.008	325	0.000	0.000	0.000	0.000	0.000	0.000	0.000	0.000
w_{rot}	0.002	0.000	0.010	313	0.000	0.000	0.000	0.000	0.000	0.000	0.000	0.000
Ts	0.770	2.695	0.984	569	18.820	4.915	30.793	6.747	17.193	3.818	27.083	8.614
var(u)_{rot}	1.013	-0.021	0.994	564	0.739	0.870	6.595	0.012	0.728	0.884	6.757	0.009
var(v)_{rot}	0.973	0.017	0.995	569	0.650	0.817	5.289	0.008	0.649	0.797	5.162	0.007
var(w)_{rot}	0.880	0.004	0.994	563	0.228	0.291	2.081	0.000	0.205	0.257	1.829	0.000
var(Ts)	0.845	0.007	0.909	564	0.143	0.134	1.053	0.002	0.127	0.119	1.183	0.003
CO_2	1.04	-0.74	0.990	588	17.009	0.761	19.603	15.714	16.868	0.722	19.214	15.622
H_2O	1.026	38.50	0.91	566	418.044	83.800	600.543	208.452	469.319	92.323	706.452	43.651
var(CO_2)	0.806	-0.001	0.955	557	0.009	0.013	0.143	0.000	0.006	0.011	0.119	0.000
var(H_2O)	1.153	3.434	0.995	556	199.517	278.693	2402.562	0.228	233.397	321.962	2679.219	0.351
w'T'	0.913	-0.001	0.986	488	0.030	0.072	0.252	-0.089	0.026	0.067	0.231	-0.086
w'CO_2'	0.544	0.000	0.851	489	-0.004	0.012	0.018	-0.038	-0.002	0.007	0.044	-0.025
w'H_2O'	1.079	-0.032	0.986	485	1.660	2.241	8.849	-0.861	1.760	2.436	10.331	-0.967
Ta-asp	1.064	-2.309	0.842	593	16.260	4.899	27.844	5.138	14.986	5.678	28.300	2.506
Ta-HMP	1.041	-2.013	0.840	593	16.332	4.999	28.288	5.016	14.986	5.678	28.300	2.506
RH-HMP	0.890	12.730	0.727	593	57.043	19.497	94.807	18.768	63.522	20.367	93.200	19.430
Pressure	0.973	2.270	0.985	568	99.440	0.312	99.996	98.780	98.982	0.306	99.600	98.300
Wind spd	1.012	-0.021	0.999	569	2.190	1.258	8.395	0.149	2.195	1.273	8.528	0.167
Wind dir	1.017	-41.528	1.000	542	182.919	89.679	355.885	0.911	161.809	93.104	358.707	0.063
SWin	1.001	1.387	0.999	322	469.022	329.618	981.046	-4.020	470.751	329.983	997.000	0.000
SWout	1.007	0.345	0.998	556	37.798	43.337	127.546	0.181	38.395	43.671	129.917	0.208
LWin	1.096	-34.831	0.954	556	307.585	26.251	370.636	242.798	302.297	29.455	374.718	236.437
LWout	0.989	9.030	0.984	593	385.928	34.560	471.432	318.463	390.772	34.469	478.368	325.893
Rnet	0.995	-1.500	0.995	593	153.074	276.383	742.194	-105.690	150.744	275.564	766.902	-115.827
SW2 diff	0.975	2.048	0.973	593	66.124	81.059	431.151	0.607	66.516	80.118	401.760	0.159
SW2 tot	0.921	-3.041	0.997	593	279.669	352.283	1012.647	0.763	254.603	325.050	952.800	0.134
PARin	0.949	-6.272	0.998	593	565.473	712.742	2059.933	0.000	530.423	677.188	1985.000	0.280
PARdiff	0.975	4.266	0.973	593	137.759	168.872	898.231	1.264	138.576	166.912	837.000	0.331
PARout	1.031	0.020	0.996	593	27.968	34.155	99.770	0.000	28.865	35.288	102.079	-0.189
CNRTemp	0.982	1.575	0.996	593	14.670	6.387	30.364	0.874	15.976	6.283	31.630	2.762

Site Name: Tonzi Ranch (US-Ton)
Visit Dates: 12 – 25 April 2016

Appendix 1 – Site information

General Site Information

Site name:	Tonzi Ranch (US-Ton)
Mean canopy height (m); provide source of measurement:	~7.5-1x (m) images
Time zone of site data acquisition?	PST
Was PEC system sync'd to their local time? When?	Yes, 2016-04-12 16:08
Sampling frequency of fast response system:	10 Hz

http://ameriflux-data.lbl.gov:8080/SitePages/siteInfo.aspx?US-Ton

Latitude (+N/-S): 38.4316 (38° 25' 53.76")
Longitude (+E/-W): -120.9660 (-120° 57' 57.5994")
Elevation: 177 m
Declination: 13.57° E on 2016-04-12

Site Instrumentation (make/model) - heights recorded below

Instrument	**Make/model**
Sonic anemometer	Gill - WMP
Fast temperature sensor	
IRGA#1 (open/closed)	LI-7500
IRGA#2 (open/closed)	
Other gas analyzer (describe)	
Radiometer#1 (specify net or which component)	CNR1 (4-component Net radiometer)
Radiometer#2 (specify net or which component)	CMP11 (Pyranometer)
Radiometer#3 (specify net or which component)	
PAR#1	PAR-lite (PAR quantum)
PAR#2	Delta-T BF5 & home-made PAR diffuse
Temp. sensor#1 (is aspirated?)	HMP-45 (mechanically aspirated)
Temp. sensor#2 (is aspirated?)	
Humidity sensor (is aspirated?)	HMP-45 (mechanically aspirated)
Barometer	
Wind sensor	
Vertical profile systems (temperature, winds, trace gases)	

Site Name: Tonzi Ranch (US-Ton)
Visit Dates: 12 – 25 April 2016

Eddy covariance details (sensor heights, orientation, separation)

	PECS	**in-situ**
Sonic anemometer		
height [m]	23.6	23.7
orientation of sensor [o]	143	38
distance from tower/tripod [m]		
orientation of boom (if different) [o]		
Open-path IRGA (measure relative to sonic)		
Vertical separation [cm] (pos if IRGA is above sonic)	-12	0
E/W separation [cm] (pos if IRGA is east of sonic)	-28	0
N/S separation [cm] (pos if IRGA is north of sonic)	-30	+35
Closed-path IRGA (measure relative to sonic)		
Vertical separation [cm] (pos if IRGA is above sonic)	-12	n/a
E/W separation [cm] (pos if IRGA is east of sonic)	+5	n/a
N/S separation [cm] (pos if IRGA is north of sonic)	-5	n/a
Inlet tube length [cm]		
Inlet tube inner diameter [mm]		
Inlet tube flow rate [lpm]		

Slow response details (sensor heights, orientation, separation

	PECS	**in-situ**
Radiometer#1 - height [m]	21.8 m	21.8 m
Radiometer#1 - orientation [o]	180	180
Radiometer#2 - height [m]	21.8	21.8
Radiometer#2 - orientation [o]	180	180
PAR - height [m]	21.8	21.8
PAR - orientation [o]	180	180
Temp. sensor#1 - height [m] (Asp)	21.7	
Temp. sensor#2 - height [m] (HMP)	22.18	21.8
Humidity sensor - height [m]	22.18	21.8
Barometer - height [m]	18.88	
Wind sensor - height [m]		

Sketch layout of setup

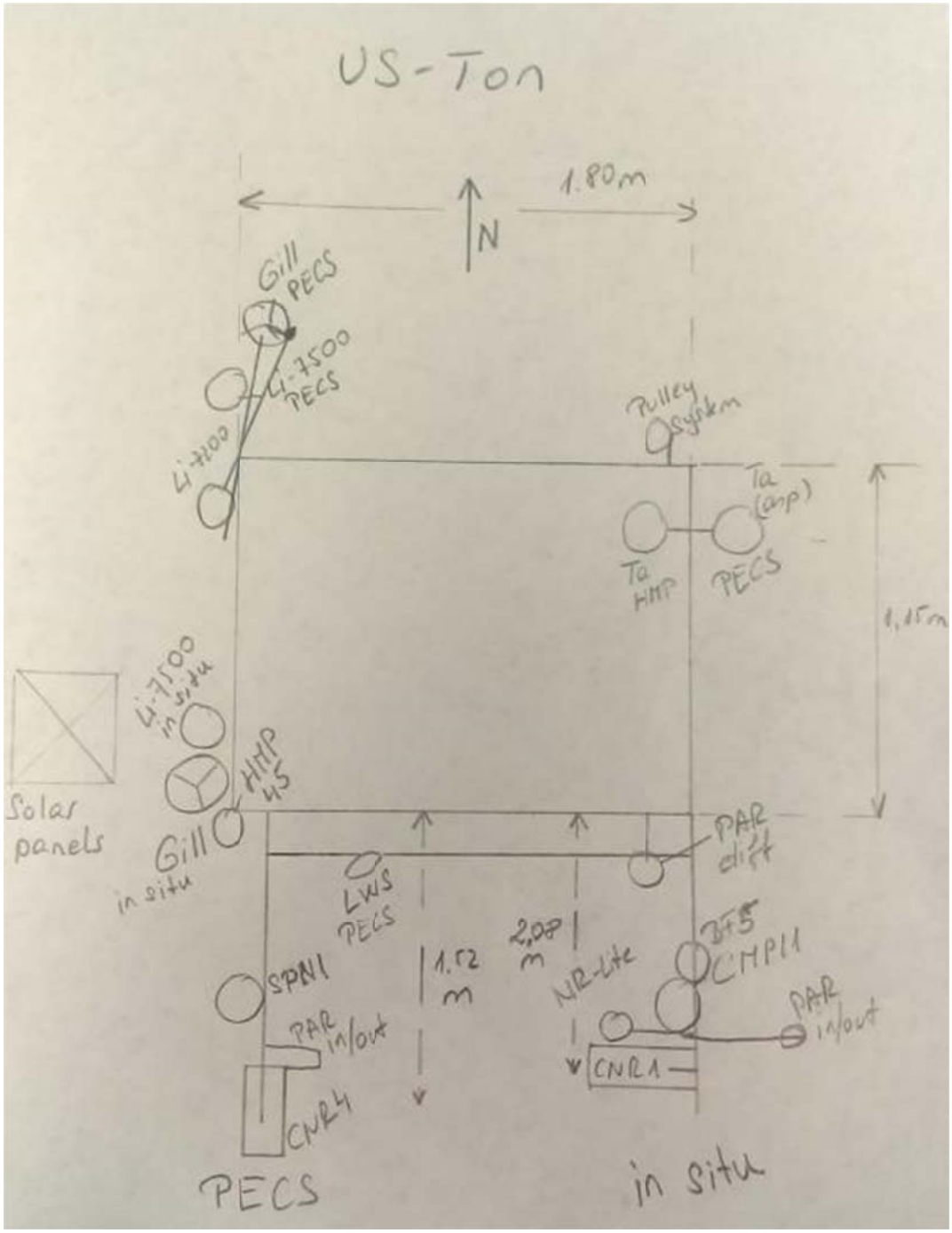

Appendix 2 – Photograph of Tonzi Ranch tower